USGS
science for a changing world

Isotropic, Anisotropic, and Borehole Washout Analyses in Gulf of Mexico Gas Hydrate Joint Industry Project Leg II, Alaminos Canyon Well 21–A

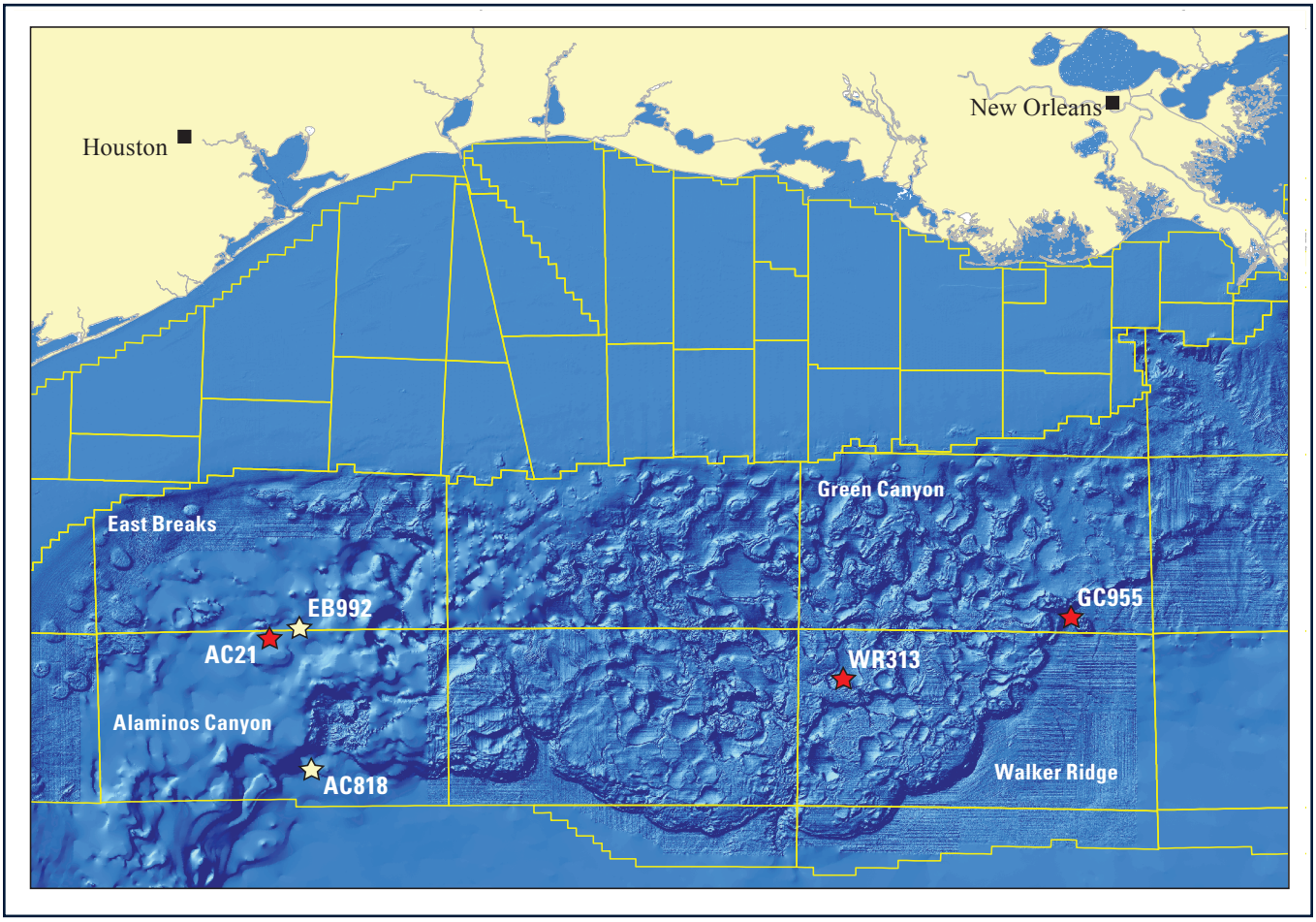

Scientific Investigations Report 2012–5046

U.S. Department of the Interior
U.S. Geological Survey

Isotropic, Anisotropic, and Borehole Washout Analyses in Gulf of Mexico Gas Hydrate Joint Industry Project Leg II, Alaminos Canyon Well 21–A

By Myung W. Lee

Scientific Investigations Report 2012–5046

U.S. Department of the Interior
U.S. Geological Survey

U.S. Department of the Interior
KEN SALAZAR, Secretary

U.S. Geological Survey
Marcia K. McNutt, Director

U.S. Geological Survey, Reston, Virginia: 2012

Suggested citation:
Lee, M.W., 2012, Isotropic, anisotropic, and borehole washout analyses in Gulf of Mexico Gas Hydrate Joint Industry Project Leg II, Alaminos Canyon well 21–A: U.S. Geological Survey Scientific Investigations Report 2012–5046, 23 p.

Contents

Figures

Table

Abbreviations Used in This Report

≈	nearly equal to
AC21–A	Alaminos Canyon 21 A well
JIP	Gulf of Mexico Gas Hydrate Joint Industry Project
KG model	model proposed by Kolterman and Gorelick (1995)
Hz	hertz
MPa	megapascal
P-wave	compressional wave
S-wave	shear wave
ft	foot
g/cm^3	grams per cubic centimeter
in.	inch
kHz	kilohertz
km/s	kilometers per second
ms	milliseconds
ohm-m	ohm-meter

Isotropic, Anisotropic, and Borehole Washout Analyses in Gulf of Mexico Gas Hydrate Joint Industry Project Leg II, Alaminos Canyon Well 21–A

By Myung W. Lee

Abstract

Through the use of three-dimensional seismic amplitude mapping, several gas hydrate prospects were identified in the Alaminos Canyon area of the Gulf of Mexico. Two of the prospects were drilled as part of the Gulf of Mexico Gas Hydrate Joint Industry Program Leg II in May 2009, and a suite of logging-while-drilling logs was acquired at each well site. Logging-while-drilling logs at the Alaminos Canyon 21–A site indicate that resistivities of approximately 2 ohm-meter and P-wave velocities of approximately 1.9 kilometers per second were measured in a possible gas-hydrate-bearing target sand interval between 540 and 632 feet below the sea floor. These values are slightly elevated relative to those measured in the hydrate-free sediment surrounding the sands. The initial well log analysis is inconclusive in determining the presence of gas hydrate in the logged sand interval, mainly because large washouts in the target interval degraded well log measurements. To assess gas-hydrate saturations, a method of compensating for the effect of washouts on the resistivity and acoustic velocities is required. To meet this need, a method is presented that models the washed-out portion of the borehole as a vertical layer filled with seawater (drilling fluid). Owing to the anisotropic nature of this geometry, the apparent anisotropic resistivities and velocities caused by the vertical layer are used to correct measured log values. By incorporating the conventional marine seismic data into the well log analysis of the washout-corrected well logs, the gas-hydrate saturation at well site AC21–A was estimated to be in the range of 13 percent. Because gas hydrates in the vertical fractures were observed, anisotropic rock physics models were also applied to estimate gas-hydrate saturations.

Introduction

In May 2009, the Gulf of Mexico Gas Hydrate Joint Industry Project Leg II (JIP Leg II) conducted logging-while-drilling operations at three sites in the northern Gulf of Mexico (fig. 1) (Collett and others, 2009). These locations were selected primarily from the three-dimensional seismic data to test geological and geophysical interpretation methods of prospecting for gas hydrate-bearing sand reservoirs (Hutchinson and others, 2009; Shedd and others, 2009). A primary scientific objective of the drilling program was to obtain high-quality logging-while-drilling data through the sand reservoir facies to further characterize the nature of gas hydrate occurrence and to refine estimates of gas hydrate content (Collett and others, 2009).

Gas hydrate prospects in Alaminos Canyon block 21 (AC21) were identified by mapping anomalous amplitude responses on three-dimensional seismic data; the anomalous responses were identified by strong peak-leading events at the top of the reservoir (Frye and others, 2009). Well log analysis of data from previously drilled industry wells in Alaminos Canyon 21–A site (AC21) and the adjacent East Breaks block 992 (EB992) (fig. 1) indicated low to moderate gas-hydrate saturations in sand reservoirs, as shown by a slightly elevated formation resistivity of ≈2 ohm-meters (ohm-m) measured at well EB992 #1 and the high-amplitude leading peak associated with the seismically defined top of an inferred sandy reservoir facies at site AC21 (Frye and others, 2009).

Resistivity and velocity well logs are generally used to estimate gas-hydrate saturations in sediments because of their elevated resistivity and velocities compared with those of water-wet sediments (Guerin and others, 1999; Collett and Ladd, 2000). However, if the well log measurements are markedly affected by large borehole washouts, then the saturation estimates are not accurate when they are computed by the currently available rock physics models, such as the Archie equation for resistivity (Archie, 1942) and the effective medium and Biot-Gassmann theories for velocity (for example, Ecker and others, 1998; Helgerud and others, 1999; Jakobsen and others, 2000; Lee, 2002a; Lee and Waite, 2008). Furthermore, because the physical properties of gas hydrate-bearing sediment at low saturation are similar to those of water-wet sediment, detecting low gas-hydrate saturations from well logs is even more difficult.

Logging-while-drilling well logs from the Alaminos Canyon 21–A (AC21–A) well indicate large borehole washouts at the target sand interval. Consequently, conventional interpretation of the well logs was inconclusive in determining whether gas hydrates are present at the AC21–A site. One of the objectives of this paper is to present

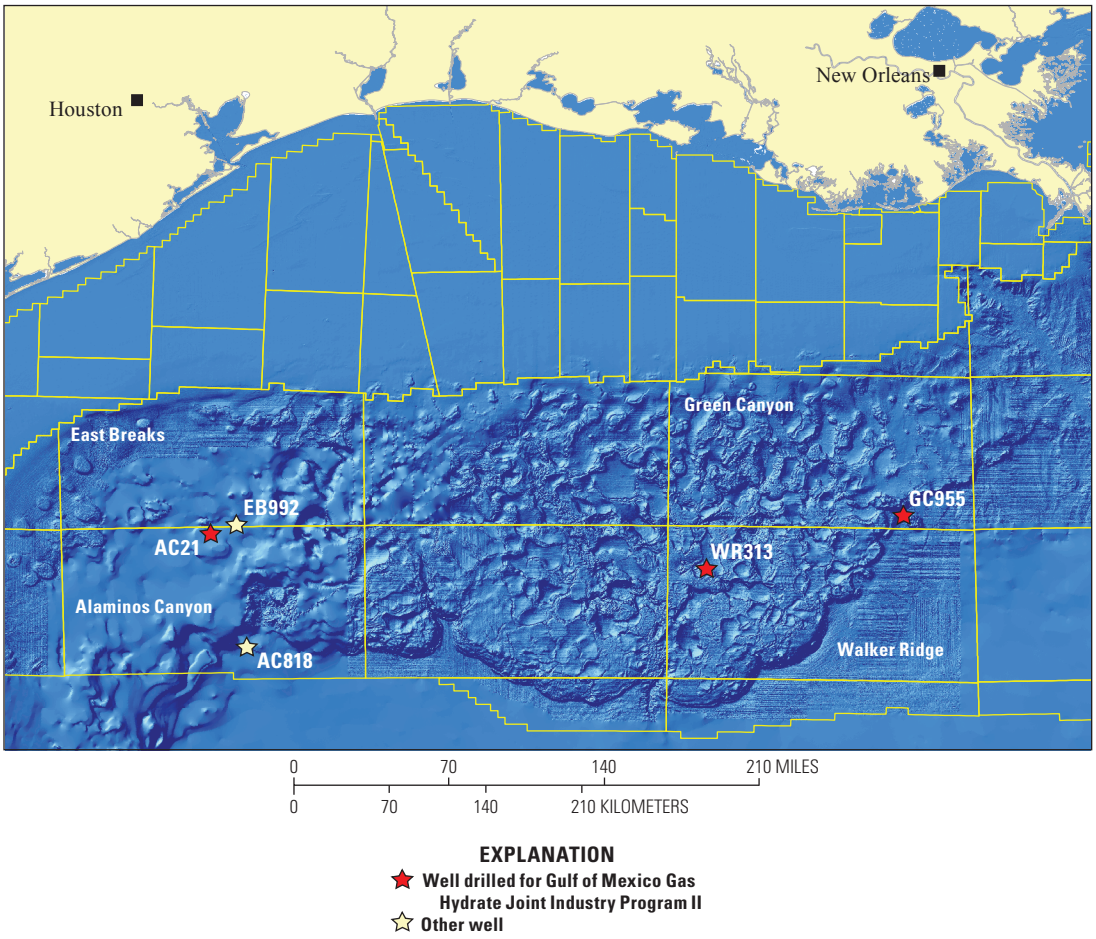

Figure 1. Location of the wells drilled for the Joint Industry Project Leg II, Gulf of Mexico. Modified from Collett and others (2009).

a method of compensating for the effects of large washouts on resistivity and velocity well log measurements. The effect of the borehole washout is modeled by using a vertical layer filled with seawater (that is, drilling fluid). In order to compensate for the washout effect on the log measurements, resistivity anisotropy (Kennedy and Herrick, 2004) and velocity anisotropy (Lee, 2009) methodologies are used. These anisotropic rock physics models are also applied to estimate gas-hydrate saturations in the vertical fractures in clay-bearing sediments. To model end-member properties of the fracture and isotropic gas-hydrate-bearing sediments, the connectivity equation for resistivity (Montaron, 2009; Lee, 2011) and a simplified three-phase equation for velocity (Lee, 2008) are used.

Estimating gas-hydrate saturations requires a value for porosity of sediment as well as values of measured resistivity and velocity. It was observed that a washout degrades the density log most severely, resulting in erroneous porosity calculations. Therefore, to calculate reasonable porosity in the washout intervals, porosity estimated from the sand-shale porosity model is used (Marion and others, 1992; Kolterman and Gorelick, 1995).

Well Logs

Well AC21–A, located at a water depth of 4,889 feet (ft), was the first location drilled at the AC21 site during the Gulf of Mexico JIP Leg II, and a suite of logging-while-drilling logs was acquired. In the analysis of this well, the caliper, gamma ray, bulk density, ring resistivity, and compressional-wave (P-wave) velocity-log data are used to assess gas hydrate occurrence and saturations in several sand reservoirs and in one fractured reservoir in clay-bearing sediments. Although shear wave (S-wave) velocities were measured, it was possible to interpret S-wave logs only in limited portions of the sedimentary section. Thus, the S-wave velocity log was used only to identify vertical fractures in clay-bearing sediments.

Well AC21–A was drilled near gauge with a diameter of ≈8.5 inches (in.) for most of the hole except for the upper 140 ft below the sea floor and in the target sand reservoirs between 540 and 632 ft below the sea floor, where caliper measurements indicate extensive borehole washout to diameters greater than 10 in. Because of this borehole enlargement, some recorded data in these intervals, particularly density, are unreliable.

The target sand was encountered at a depth of 540 ft below the sea floor, which is within the gas-hydrate stability zone (Frye and others, 2009). The gross target interval consists of two sand units separated by a 15-ft shale break. The upper sand unit is 15 ft thick and has a sharp base and top. The lower sand unit is 62 ft thick, contains a sharp base, and slightly fines upward to the top. The total gross thickness of the sand is 77 ft, and the ratio of sand to shale for both of the target sands is high (Frye and others, 2009).

Sand-Shale Porosity Model

The logging-while-drilling logs indicate large washouts within gamma log-inferred sand intervals, where little or no gas hydrate is speculated to occur. In these washed-out intervals all logs, except the gamma ray log, appeared to be markedly degraded. The porosities derived from the density logs are greater than 0.8 for some intervals, which is not reasonable. Because no nearby wells had density logs that could help with porosity estimation, it is important to correct the porosity data within the washed-out section of the borehole or to estimate reasonable porosities in the unlogged intervals, in order to analyze in detail the resistivity and acoustic logs and, in turn, to estimate gas-hydrate saturations.

Marion and others (1992) proposed a sand-shale porosity model to estimate porosity from the shale or clay volume of the sediments. This model is based on a microgeometrical model for mixtures of sand and clay. For sand and shaly sands in which clay is dispersed in the pore space of the load-bearing sand, the porosity is reduced by the clay. In contrast, for shales and sandy shales in which sand grains are dispersed in a clay mixture, porosity increases by the contribution of bound water in the clay. Marion's (1992) model, however, underestimates porosities of clay-rich sediments. To compensate for the underestimation of the porosity, Kolterman and Gorelick (1995) modified the Marion model (the modified model is referred to as the KG model in this paper).

The KG model is used in this investigation to relate the shale volume to the porosity of the sediment. The porosities are given by

$$\phi = \phi_{sand} - yV_{sh}(1-\phi_{shale}) + (1-y)V_{sh}\phi_{shale} \text{ for } V_{sh} < \phi_{sand} \quad (1a)$$

where

$$y = V_{sh}(y_{min} - 1)/\phi_{sand} + 1$$

and by

$$\phi = \phi_{shale}V_{sh} + \phi_{sand}(1-y) \text{ for } V_c \geq \phi_{sand} \quad (1b)$$

where

$$y = (V_{sh} - 1)\,(1 - y_{min})/(1 - \phi_{sand}) + 1,$$

and where

ϕ_{sand} is the sand porosity,

ϕ_{shale} is the shale porosity,

and

V_{sh} is the shale volume estimated from the gamma ray log.

The values of y_{min} depend on the effective pressure and were determined experimentally to be 0.76 at a pressure of 0 megapascals (MPa) and 0.8 at 50 MPa (Koltermann and Gorelick, 1995). Pratson and others (2003) used $y_{min} = 0.78$ to model porosities of sediments in the Amazon Fan.

Figure 2*A* shows calculated porosity with respect to shale volume by using equations 1a and 1b with $\phi_{sand} = 0.42$ and $\phi_{shale} = 0.7$ and with two values of y_{min}, 0.78 and 1.0. As shown in figure 2*A*, porosity decreases as shale volume increases until the fraction of shale volume matches sand porosity. If the shale volume is greater than the sand porosity, porosity increases as shale volume increases, because the porosity contributed by clay-bound water also increases. The estimated porosity with $y_{min} = 1$ (Marion's model) is less than that of the KG model for all ranges of shale volumes.

Figure 2*B* shows porosities derived from the measured density log and estimated porosities derived by using the KG model with $\phi_{sand} = 0.42$, $\phi_{shale} = 0.65$, and $y_{min} = 0.7$. The porosity derived from the density log ranges from 0.3 to 0.8, and the high porosities observed between 540 and 632 ft below the sea floor are caused by the borehole washout. By using the KG model, an average porosity of 0.38 is calculated for the sand interval, which more closely agrees with that by Gregory (1977) and Zimmer (2003). Therefore, in the following analysis, the porosity of the sand interval is replaced with that calculated by using the KG model.

Isotropic Rock Physics Models

Isotropic Resistivity

Montaron (2009) introduced a connectivity equation to model resistivity of non-Archie rocks, and this equation is used in this report**.** The electrical resistivity of sediments (R_t) can be expressed by using the connectivity equation, including the shale effect, as follows (Lee, 2011):

$$R_t = \frac{aR_w}{\left(S_w\phi - \chi_w\right)^{\mu}} \quad (2)$$

where a, S_w, R_w, μ, and χ_w are the conventional Archie parameter, water saturation, resistivity of connate water, connectivity exponent, and water connectivity correction index, respectively. The resistivity of clean sand is given by equation 2 with $\chi_w = 0$. The magnitude of χ_w, which indicates the degree of clay or shale effect on electrical resistivity, is given by the following equation (Lee, 2011):

$$\chi_w = \lambda V_{sh}\phi^{\mu}S_w \quad (3)$$

where

λ is an adjustable parameter.

This parameter can be estimated by calculating the resistivity of water-saturated sediments by substituting equation 3 into equation 2 and then by adjusting λ until there is satisfactory agreement between the calculated and measured resistivities of water-saturated sediments.

The resistivity of gas-hydrate-bearing sediment (R_t) with saturation S_h ($S_h = 1 - S_w$) can be expressed by using the water-filled porosity (ϕ_w) in the following way:

$$R_t = \frac{aR_w}{\left(\phi_w - \chi_w\right)^{\mu}} \tag{4}$$

where

$$\phi_w = S_w\phi = (1 - S_h)\phi.$$

Isotropic Velocity

The velocities of isotropic gas-hydrate-bearing sediment, whereby gas hydrate fills sediment pore space, can be calculated by using a simplified three-phase equation as given by Lee (2008). Lee (2008) derived the bulk (k) and shear (μ) moduli of gas-hydrate-bearing sediment at low frequencies (that is, for well log and seismic data) as follows:

$$k = K_{ma}(1 - \beta_p) + \beta_p^2 K_{av} \tag{5}$$

$$\mu = \mu_{ma}(1 - \beta_S)$$

with

$$\frac{1}{K_{av}} = \frac{\beta_p - \phi}{K_{ma}} + \frac{\phi_w}{K_w} + \frac{\phi_h}{K_h}, \tag{6}$$

$$\beta_p = \frac{\phi_{as}(1+\alpha)}{(1+\alpha\phi_{as})}, \text{ and } \beta_s = \frac{\phi_{as}(1+\gamma\alpha)}{(1+\gamma\alpha\phi_{as})}$$

$$\phi_{as} = \phi_w + \varepsilon\phi_h, \phi_w = (1 - S_h)\phi, \text{ and } \phi_h = S_h\phi.$$

where

α is the consolidation parameter (Pride and others, 2004; Lee, 2005),

γ is a parameter related to shear modulus given by $\gamma = (1 + 2\alpha)/(1 + \alpha)$;

K_{ma}, K_w, and K_h are the bulk moduli of sediment grains, water, and gas hydrate respectively;

and

μ_{ma} is the shear modulus of the grains.

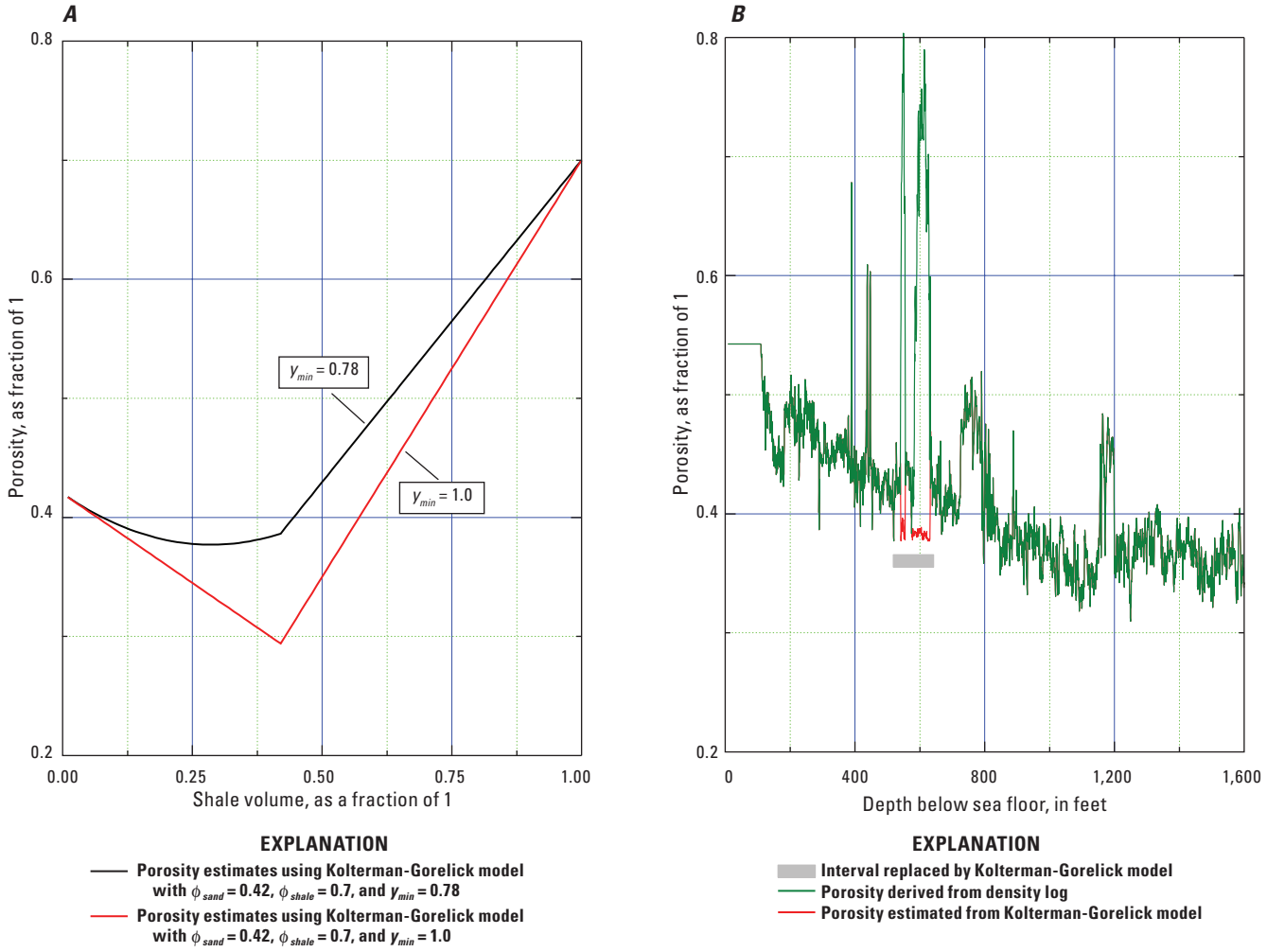

Figure 2. *A*, Porosity estimated from a sand-shale porosity model by Kolterman and Gorelick (1995). *B*, Porosities derived from the measured density log and replaced porosity estimated from the sand-shale-mixture model.

The parameter ε is a constant that accounts for the reduced effect of hydrate formation relative to compaction in terms of sediment stiffening. Lee and Waite (2008) recommended using a value of $\varepsilon = 0.12$ for modeling velocities of gas-hydrate-bearing sediment.

The choice of $\varepsilon = 0.12$ is based on gas-hydrate saturation less than about 85 percent (Lee and Waite, 2008). Generally, gas-hydrate saturations in sands are less than 85 percent because of capillary water in the pore spaces, so the choice of $\varepsilon = 0.12$ is widely accepted. However, as gas-hydrate saturation approaches 100 percent of pore space, the bulk and shear moduli of the gas-hydrate-bearing sediment approach Hill's (1952) average. However, the bulk and shear moduli predicted from the simplified three-phase equation for 100 percent gas hydrate differ from those of Hill's average. Therefore, if the simplified three-phase equation is extended to gas-hydrate saturation of more than 85 percent, some modification of ε is required.

The P-wave (V_p) velocity and the S-wave velocities (V_s) of the gas-hydrate-bearing sediment are given by

$$V_p = \sqrt{\frac{k + 4\mu/3}{\rho_b}} \text{ and } V_s = \sqrt{\frac{\mu}{\rho_b}} \tag{7}$$

where

ρ_b is the bulk density of the gas-hydrate-bearing sediment, which is given by

$$\rho_b = \rho_s(1-\phi) + \rho_w\phi(1-S_h) + \rho_h\phi S_h.$$

For water-saturated sediments, the simplified three-phase equation is the same as the Gassmann equation.

The consolidation parameter α in equation 6 depends on the effective pressure and degree of consolidation of sediments. Mindlin (1949) showed that the bulk and shear moduli depend on the ⅓ power of effective pressure. On the basis of this theory by Mindlin (1949), the depth-dependent or effective-pressure-dependent α is given by the following equation:

$$\alpha_i = \alpha_0(p_0/p_i)^\beta \approx \alpha_0(d_0/d_i)^\beta \tag{8}$$

where

α_0 is the consolidation parameter at the effective pressure p_0 or at depth d_0

and

α_i is the consolidation parameter at the effective pressure p_i or at depth d_i.

These parameters can be estimated from the porosities and velocities of water-saturated sediments (Lee, 2006).

Anisotropic Rock Physics Models

Anisotropic Resistivity

Let medium 1 be a fracture filled with gas hydrate and medium 2 be water-saturated sediments surrounding the fracture. Let ϕ_1, μ_1, α_1, χ_{w1}, and S_{w1} be porosity, connectivity exponent, Archie parameter, connectivity correction index, and water saturation for medium 1, respectively, and let ϕ_2, μ_2, α_2, χ_{w2}, and S_{w2} be the corresponding parameters for medium 2. The volume of the fracture is given by η and the volume of sediment is given by $1 - \eta$. By using anisotropic equations of Kennedy and Herrick (2004), the formation factor F ($F = R_t / R_w$) that is parallel to the fracture or horizontal fracture (F_h) and perpendicular to the fracture or vertical fracture (F_v) are given by the following equations:

$$F_h = \frac{1}{\eta(\phi_{w1} - \chi_{w1})^{\mu_1}/a_1 + (1-\eta)(\phi_{w2} - \chi_{w2})^{\mu_2}/a_2} \tag{9}$$

$$F_v = \frac{(1-\eta)(\phi_{w1} - \chi_{w1})^{\mu_1}/a_1 + \eta(\phi_{w2} - \chi_{w2})^{\mu_2}/a_2}{(\phi_{w1} - \chi_{w1})^{\mu_1}(\phi_{w2} - \chi_{w2})^{\mu_2}/(a_1 a_2)} \tag{10}$$

where ϕ_{w1} and ϕ_{w2} are water-filled porosities for media 1 and 2, respectively. In this report it is assumed that $a_1 = a_2 = 1$, which is generally true for clean sands. This assumption is also accurate for the logging-while-drilling logs acquired during Gulf of Mexico JIP Leg II.

Assume that the strike of the fracture is in the y-direction in the Cartesian coordinate system and that z is the vertical direction. For an arbitrary dip angle θ of the fracture from the horizontal axis, the tensor formation factor (F_{ij}) can be written as follows:

$$F_{ij} = \begin{bmatrix} \cos\theta & 0 & \sin\theta \\ 0 & 1 & 0 \\ -\sin\theta & 0 & \cos\theta \end{bmatrix} \begin{bmatrix} F_h & 0 & 0 \\ 0 & F_h & 0 \\ 0 & 0 & F_v \end{bmatrix} \begin{bmatrix} \cos\theta & 0 & -\sin\theta \\ 0 & 1 & 0 \\ \sin\theta & 0 & \cos\theta \end{bmatrix} \tag{11}$$

The measured resistivity for the analysis in this report can be represented by F_{11} or F_{xx} and is given by

$$F_{xx} = F_h\cos^2\theta + F_v\sin^2\theta. \tag{12}$$

The formation factor or resistivity of a fracture filled with gas hydrate is modeled as follows. It is assumed that the porosity of the open fracture is equal to 1. As the gas hydrate accumulates in the open fracture, the water-filled porosity decreases. At 100 percent gas-hydrate saturation, porosity is equal to zero. However, zero porosity cannot be used in equation 10 to have a finite formation factor. Therefore, it is assumed that a certain amount of water-filled porosity remains in the fracture model (ϕ_{w1} in equations 9 and 10). In other words, the fracture is filled with gas hydrate with a saturation of $(1 - \phi_{w1})$. Because open fractures contain no shale, it is assumed that $\chi_{w1} = 0$ and $\mu_1 = 2$. The magnitude of the formation factor for a fracture, therefore, depends on ϕ_{w1}, and a representative porosity for the fracture model should be established. Note that ϕ_{w1} is not actual porosity in the fracture but is a convenient parameter here used to analyze resistivity by using a fracture model. A judicious choice of ϕ_{w1} is important to accurately estimate gas-hydrate saturations by using a fracture model, so some guidelines for choosing ϕ_{w1} are helpful. For example, the formation factor of end member 1 with $\phi_{w1} = 0.05$ is 400, whereas with $\phi_{w1} = 0.035$ it is 816. Therefore, by comparing measured resistivity with various ϕ_{w1}, an optimum value can be chosen (M.W. Lee and T.S. Collett, unpub. data, 2011).

The parameters for medium 2 are those for the water-saturated sediments surrounding the fracture, which are $\phi_{w2} = \phi_2$ ($S_w = 1$) and $\mu_2 = 2$. The term χ_{w2} is estimated by using equation 3 to fit the measured resistivity of water-saturated sediments.

The connectivity index μ for an anisotropic medium can be calculated by using the method of Kennedy and Herrick (2004), and this approach was used in Lee and Collett (2009a) to analyze the fracture reservoir in Krishna Basin, India. However, μ for the anisotropic model is a function of gas-hydrate saturation (Lee and Collett, 2009a), so it is not practical to use; instead, inverse modeling is used to estimate gas-hydrate saturation for the anisotropic medium. The essence of this method is to find the fracture volume by minimizing the difference between the measured and calculated anisotropic formation factor by using equation 12 for a given dip angle of the fracture.

Anisotropic Velocity

A fracture filled with gas hydrate is modeled as layered media with two components (Lee, 2009). The first component is a fracture filled with 100 percent gas hydrate, and its characteristics are given by P-wave velocity (V_{P1}), S-wave velocity (V_{s1}), and density (ρ_1). The second component is isotropic sediment with P-wave velocity (V_{P2}), S-wave velocity (V_{s2}), and density (ρ_2). Like the resistivity model, η and $(1 - \eta)$ are the volume fraction of component 1 and volume fraction of component 2, respectively. Owing to the geometry of this model, the fracture media can be modeled as having transversely isotropic properties. Phase velocities of the transversely isotropic media caused by fractures can be computed by using the following definition:

$$<G> \equiv (\eta G_1 + (1 - \eta)G_2). \quad (13)$$

$$< \frac{1}{G} >^{-1} \equiv \left(\frac{\eta}{G_1} + \frac{(1-\eta}{G_2} \right)^{-1}$$

where

G is any elastic constant—such as the density of component 1 and of component 2.

The P- and S-wave velocities of the transversely isotropic media can be calculated from the following equations by using Lamé constants λ and μ (White, 1965):

$$A = < \frac{4\mu(\lambda+\mu)}{(\lambda+2\mu)} > + < \frac{1}{(\lambda+2\mu)} >^{-1} < \frac{\lambda}{(\lambda+2\mu)} >^2 \quad (14)$$

$$C = < \frac{1}{(\lambda+2\mu)} >^{-1}$$

$$F = < \frac{1}{(\lambda+2\mu)} >^{-1} < \frac{\lambda}{\lambda+2\mu} >$$

$$L = < \frac{1}{(\mu)} >^{-1}$$

$$N = <\mu>$$

$$\rho = <\rho>$$

$$V_p = \left(\frac{A\sin^2\varphi + C\cos^2\varphi + L + Q}{2\rho} \right)^{1/2}$$

$$V_s^V = \left(\frac{A\sin^2\varphi + C\cos^2\varphi + L - Q}{2\rho} \right)^{1/2}$$

$$V_s^H = \left(\frac{N\sin^2\varphi + L\cos^2\varphi}{\rho} \right)^{1/2}$$

$$Q = \sqrt{\left[(A-L)\sin^2\varphi - (C-L)\cos^2\varphi \right]^2 + 4(F+L)^2 \sin^2\varphi\cos^2\varphi}$$

where

φ is the angle between the wavefront normal and the vertical axis (perpendicular to the layering),

V_P is the anisotropic P-wave velocity,

V_S^H is the horizontally polarized S-wave (SH) velocity,

and

V_S^V is the vertically polarized S-wave (SV) velocity.

To model the fractured media, the horizontally polarized shear-wave velocity is used. Except for vertical and horizontal ray angles, the group velocities differ from the phase velocities; the relation between the two velocities is given in Lee (2009).

Washout Modeling

Because the washout enlarges the borehole diameter and in-place sediment is replaced by drilling fluid (seawater in this case), the borehole washout can be approximated by a vertical layer filled with drilling fluid as explained in the following material. Figure 3*A* shows a washed-out borehole with an electrical resistivity logging tool showing the source and the receiver. Because a current travels through the borehole fluid and sediment, the effect of a washout on electrical resistivity is approximately calculated by using the schematic diagram shown in figure 3*B*. In other words, the washed-out portion of the borehole is replaced by a vertical column of fluid. The resistivity and velocity responses due to a vertical fluid layer in sediments are similar to those from vertical fractures filled with fluid. Therefore, the effect of a borehole washout is here modeled by using a vertical fracture. The model is applied to both resistivity and acoustic measurements, although the acoustic log measurement is relatively more complicated than the resistivity log measurement, and it results in both resistivity and velocity anisotropy. In summary, the effect of the borehole washout on the resistivity and velocity logs is modeled by assuming anisotropic physical properties caused by a vertical fracture filled with fluid.

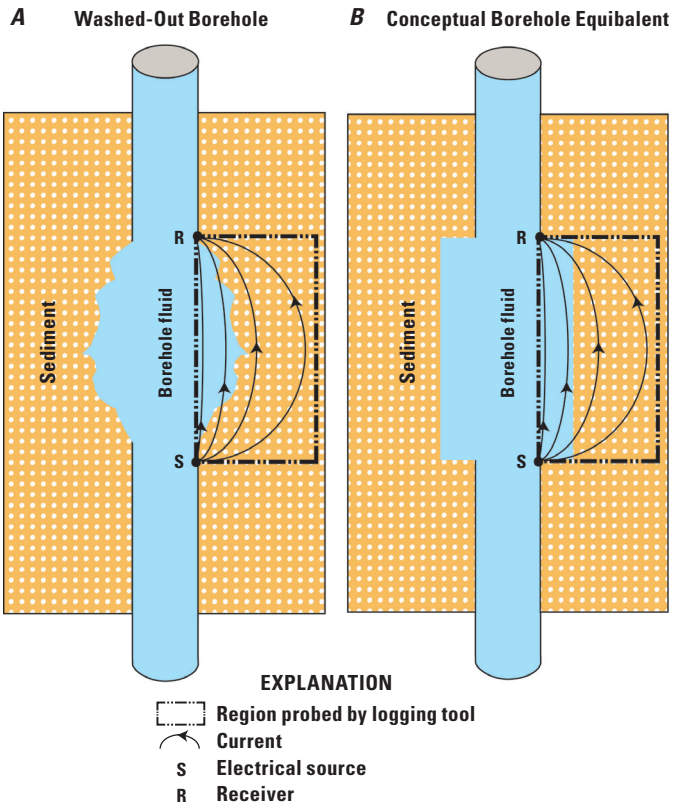

Figure 3. Borehole washout correction for an electrical resistivity tool. *A*, Washed-out borehole. *B*, Equivalent borehole configuration approximated to account for washed-out portion of borehole.

In order to accurately account for the washout effect on resistivity and velocity, a numerical modeling approach using variable shapes of the washouts would be more appropriate. However, such an approach is beyond the scope of this study, so a simple and approximate vertical fracture model is proposed. The proposed model is intended to semiquantitatively assess the effect of the washout on measured log values and to explain the abnormal log values in the washed-out intervals.

Electrical Resistivity Modeling

As discussed in the previous section, the effect of a large washout on well log measurements can be modeled as a vertical fracture filled with drilling fluid or, in this case, with seawater. By using equation 10, the resistivity R_o for water-saturated sediments in the presence of a washout filled with seawater is given by the following equation:

$$R_o = (1 - V_{wash}) \frac{R_w}{(\phi - \chi_w)^{\mu}} + V_{wash} R_{sw} \quad (15)$$

where

R_{sw} is the resistivity of seawater

and

V_{wash} is the volume fraction of the washout, which is equivalent to η in equation 10.

For the washout model, $\phi_{w1} = 1$, $\chi_{w1} = 0$, and the resistivity of the seawater is explicitly included in equation 15. The last term in equation 15 represents the contribution of seawater invaded into the washout zone on the resistivity. If $V_{wash} = 1$, the logging tool measures the resistivity of seawater. On the other hand, if $V_{wash} = 0$, the true formation resistivity (which is isotropic) is measured.

To a first-order approximation, it is assumed that V_{wash} is proportional to the amount of sand in the formation such that

$$V_{wash} = \delta(1 - V_{sh})^3 \text{ for } V_{sh} < V_{th} \quad (16)$$

$$V_{wash} = 0 \text{ for } V_{sh} = < V_{th}$$

where

V_{th} is a threshold shale volume fraction

and

V_{sh} is the shale volume fraction.

Equation 16 is based on the relation between the lithology and the size of the washout observed during Gulf of Mexico JIP Leg II—that is, the volume of washout is proportional to the volume of sand present in the formation. In other words, in clean sands large washouts were observed, whereas in shaly parts of the formation only small or no washouts were observed. The constant δ, which is related to the volume of the washout, is determined by fitting the general trend of the resistivity (calculated by using equation 15) to the measured resistivity, particularly for clean sand intervals containing no gas hydrate. The parameter δ depends on the depth of investigation of the tool relative to the washout zone as well as on lithology.

Determining the effect of a washout on electrical resistivity is straightforward because, as equation 15 indicates, resistivity decreases linearly as the volume of the washout (V_{wash}) increases (fig. 4). To calculate the resistivity of pore water, a thermal gradient of 25 degrees Celsius (°C) per kilometer with a sea floor temperature of 4°C was assumed (Frye and others, 2009). The resistivity of pore water with a salinity of 35 parts per thousand is calculated by using Arp's formula (Arp, 1953).

A washout substantially decreases measured resistivity, which approaches the resistivity of seawater as the size of the washout increases (fig. 4). The resistivity log at the Gulf of Mexico East Breaks 992 well (fig. 1) indicates that the resistivity of clean sand is close to that of seawater (0.25 ohm-m) (Frye and others, 2009), which implies that the sand interval is completely washed out.

Velocity Modeling

Similar to the gas-hydrate-filled fracture model by Lee (2009), the P- and S-wave velocities of a fracture filled with seawater can also be modeled as layered media with two components by using equations 13 and 14. In this case, the model consists of a fracture filled with 100 percent seawater and isotropic sediment. The characteristics of the fracture are given

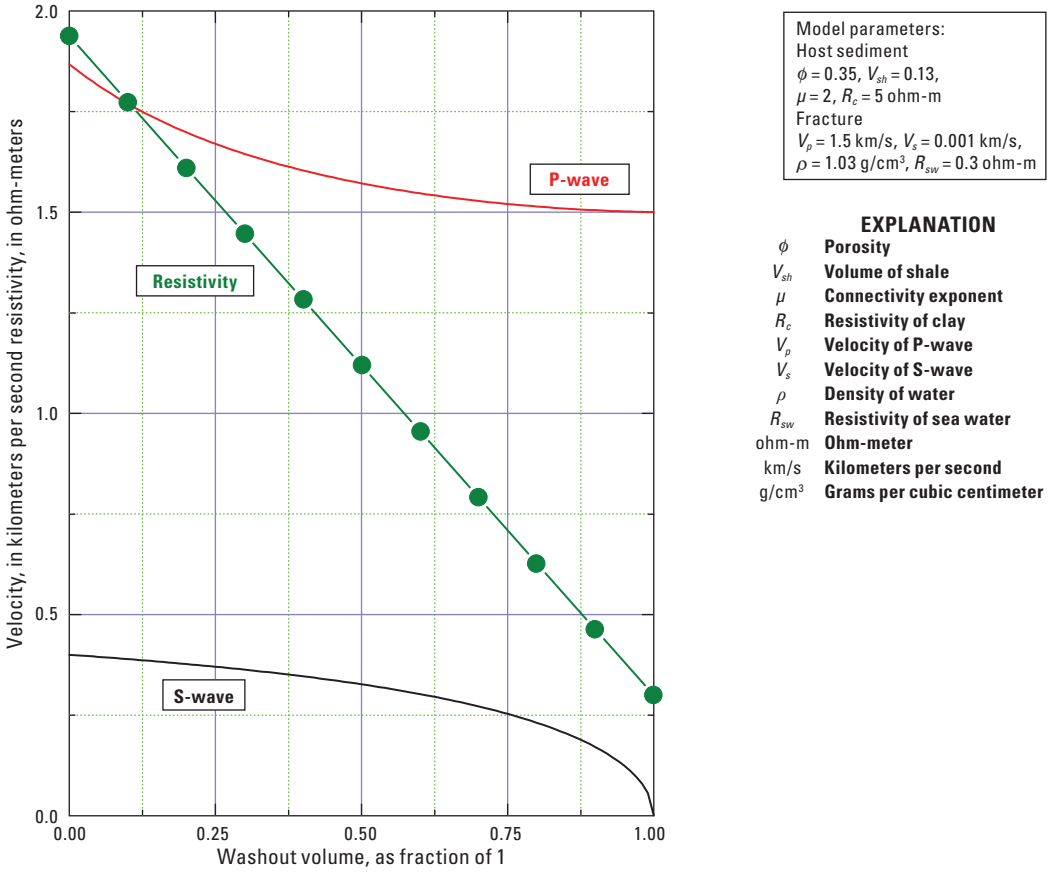

Figure 4. Effect of borehole-washout volume on resistivity and on P- and S-wave velocities in an anisotropic model produced by sediments containing a vertical, seawater-filled fracture.

by P-wave velocity (V_{P1}), S-wave velocity (V_{s1}), and density (ρ_1), and the characteristics of the sediment are given by P-wave velocity (V_{P2}), S-wave velocity (V_{s2}), and density (ρ_2).

For a washout model, velocities can be simplified by using equation 14 with $\varphi = \pi / 2$ as follows:

$$V_p = \left(\frac{A}{\rho}\right)^{1/2} \text{ and } V_S \equiv V_S^H = \left(\frac{N}{\rho}\right)^{1/2} \quad (17)$$

Figure 4 shows the effect of the size of the washout on the P- and S-wave velocities if we assume that the source and receiver of the logging tool are located in the sediment of the borehole (that is, not in a washed-out section). If the source or receiver is located in fluid, then S-wave velocity becomes zero, because shear waves cannot propagate in fluid. The model parameters used in generating figure 4 are as follows: for the water-filled fracture, V_{p1} = 1.5 kilometers per second (km/s), V_{s1} = 0.001 km/s, ρ_1 = 1.03 grams per cubic centimeter (g/cm³), and for the host sediment, V_{p2} = 1.864 km/s, V_{s2} = 0.4 km/s, and ρ_2 = 2.08 g/cm³. In contrast to the effects of a washout on electrical resistivity, the effects of a washout on velocity are more complex and nonlinear. Furthermore, the rate of velocity decrease due to the washout is greatest at low washout volumes for P-wave velocity but is greatest at high washout volumes for S-wave velocity.

Well Log Analysis

Isotropic Analysis

Measured resistivities for well AC21–A are shown in figure 5. The interval labeled “sand reservoir” is the main target sand zone and is mappable on seismic sections throughout a large area in the Gulf of Mexico Alaminos Canyon and East Breaks, as shown in Frye and others (2009). The interval labeled “fractured reservoir” is an unexpected gas hydrate accumulation in the clay-bearing sediments at this well, which is interpreted as gas hydrate filling the vertical fractures as explained later in this section.

Figure 5*A* shows the calculated resistivity of water-saturated sediment (that is, the baseline resistivity) by using the connectivity equation with μ = 2 and λ = –0.01, and by assuming that no washout is present. The calculated resistivity of about 1.8 ohm-m near 600 ft is slightly less than the measured value of 2 ohm-m. The model that assumes no washout indicates that there is a small amount of gas hydrate in the target zone (fig. 5*A*; green area at bottom). However, estimated gas-hydrate saturations in the model that assumes no washout in the “fractured reservoir” are in the range of 20–30 percent of the pore space.

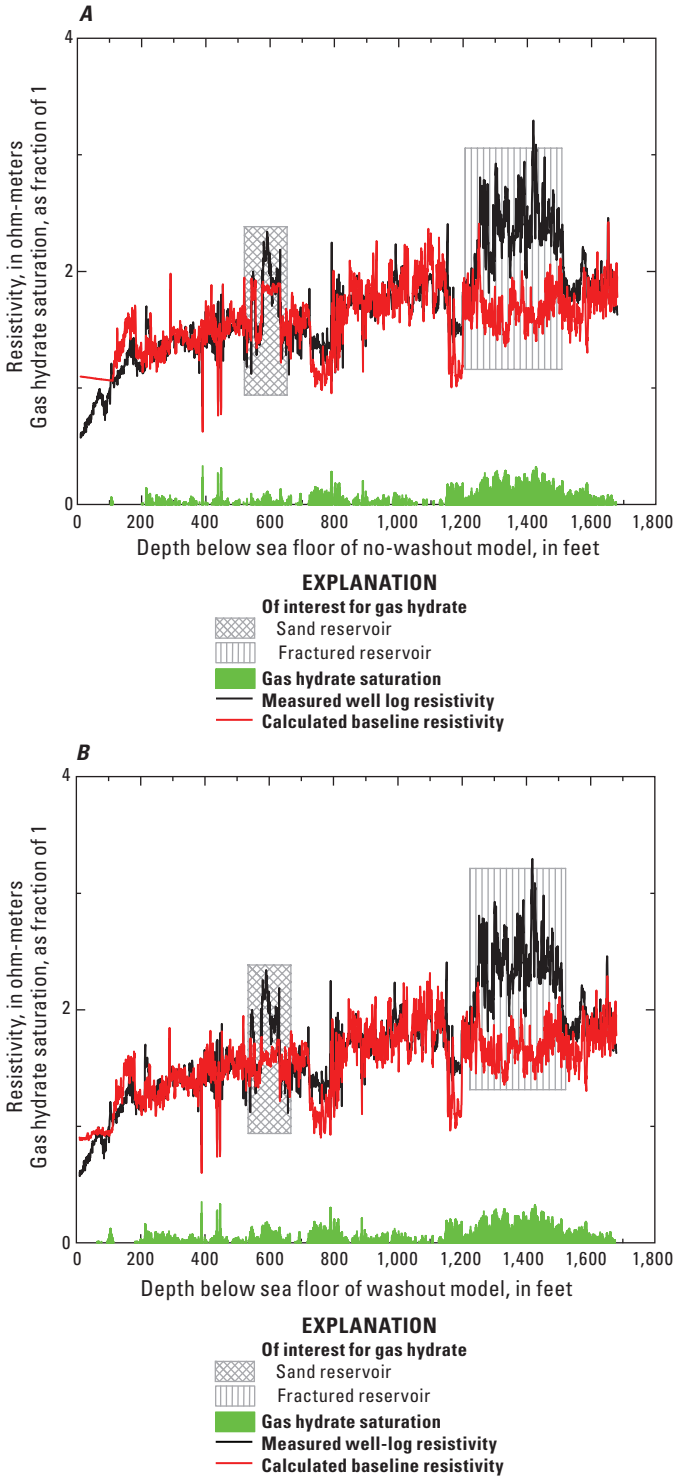

Figure 5. Measured and calculated resistivity logs of two models for Gulf of Mexico well site AC21–A and calculated gas-hydrate saturations. *A*, Model with no washout; *B*, Model with a washout. Calculated gas-hydrate saturations are also shown for each model.

Figure 5*B* shows the calculated resistivity of water-saturated sediments by using the connectivity equation with $\mu = 2$ and $\lambda = -0.01$ and by assuming the presence of a seawater-filled washout such that $\delta = 0.3$ and $V_{th} = 0.5$ in equation 16. The calculated resistivity of about 1.5 ohm-m near 600 ft is moderately smaller than the measured resistivity. The estimated gas-hydrate saturation for this model (fig. 5*B*, green area at bottom) indicates moderate gas-hydrate saturations (about 15–20 percent) throughout the sand reservoir. In the fractured interval, gas-hydrate saturations and the calculated baseline resistivities are almost the same as those shown in figure 5*A* because, according to equation 16, the washout effect on clay-bearing sediments is negligible.

Figure 6*A* shows the measured P-wave velocity with the calculated baseline velocity, if one assumes no washout and the elastic properties shown in table 1. The baseline velocities were calculated by using $\alpha = 110(300/d)^{1.1}$ with the modified porosity shown in figure 2*B* and the clay volume calculated from the shale volume as $C_v = 0.6V_{sh}$ (Hearst and others, 2000). The calculated baseline velocities (velocities of water-saturated sediments) agree reasonably well with the measured velocities except within the target sand zone, where calculated P-wave velocities are for the most part slightly higher than measured velocities. Because of the large washout in the sand interval, measured P-wave velocities were greatly reduced by the water and were less than those of the true formation velocities. The gas-hydrate saturations estimated from the P-wave velocities are negligible except for a couple of isolated intervals. The gas-hydrate saturations estimated from the P-wave velocities in the fractured interval are substantially less than those estimated from resistivities.

Figure 6*B* shows the measured P-wave velocity along with the calculated baseline velocity if one assumes that washouts have affected the measured P-wave velocity. The parameters used to model the washout are $\delta = 0.4$ and $V_{th} = 0.5$ in equation 16. The calculated baseline velocities agree reasonably well with the measured velocities except at the target sand zone, where the calculated velocities are noticeably less, by about 0.3 km/s, than the measured velocities throughout the sand reservoir. This difference implies that the washout correction on the P-wave velocity is reasonable if the sand is saturated with water and is a conservative estimate if the sand is saturated with gas hydrate.

The gas-hydrate saturations estimated from the P-wave velocities are as much as 30–35 percent in some intervals but small overall. The high gas-hydrate saturations estimated for parts of the reservoir are caused by overcorrection of the washout effect. It was observed during the Gulf of Mexico JIP Leg II that sands containing moderate amounts of gas hydrate in pore spaces and clay-bearing intervals were less apt to wash out. Because the washout correction is based on the amount of sand present in the formation, the correction for the intervals containing gas hydrate would have been overcorrected. The gas-hydrate saturations estimated in the fractured interval are similar to those shown in figure 6*A* and much less than those estimated from the resistivity.

In summary, by accounting for the borehole washout on the basis of measured resistivity and P-wave velocities, the sand interval between 540 and 632 feet below the sea floor could contain a small amount of gas hydrate with

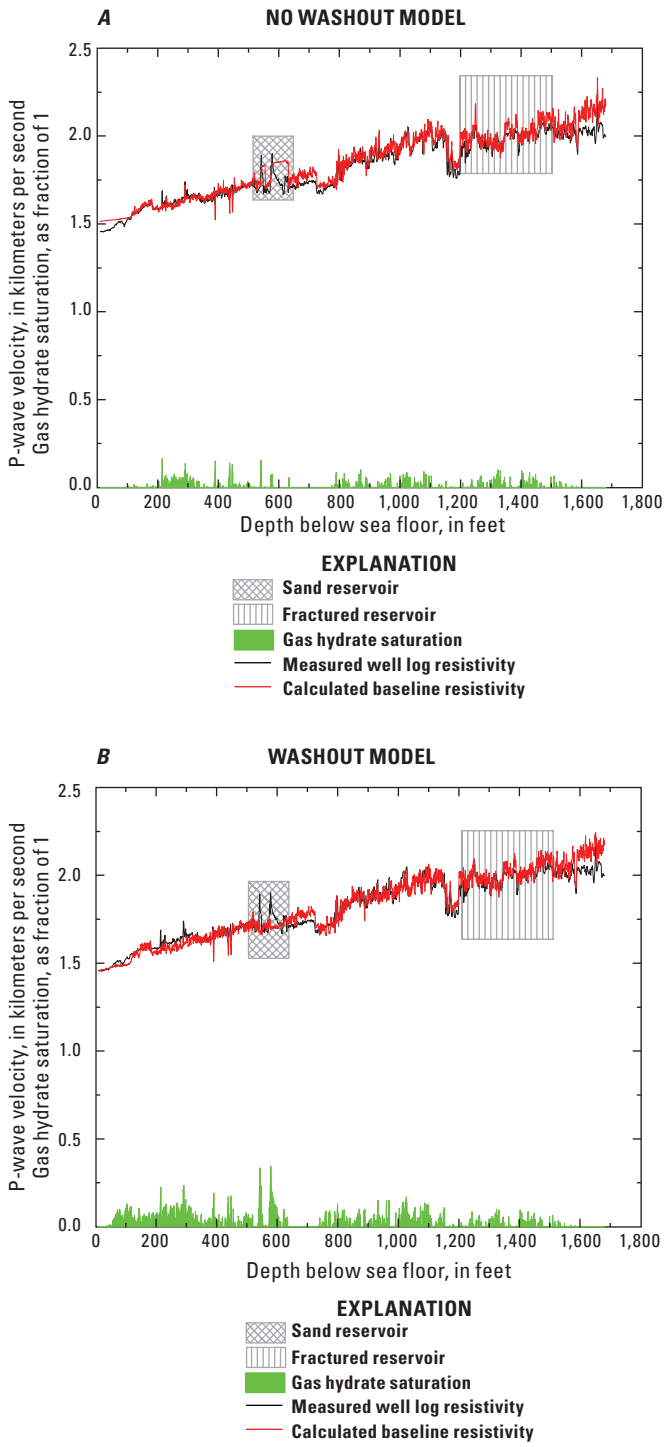

Figure 6. Measured and calculated P-wave velocity logs and gas-hydrate saturations from Gulf of Mexico well site AC21–A. *A*, Model with no washout; *B*, Model with a washout.

saturations less than about 20 percent. For vertical fractures, gas-hydrate saturations estimated from the resistivities are much higher than those estimated from the P-wave velocities. As discussed later, this difference is characteristic of vertical fractures containing gas hydrate. Although anisotropic modeling is utilized to correct for the borehole-washout effect, the gas-hydrate saturations shown in figures 5*B* and 6*B* are estimated by assuming that the gas hydrate reservoir is isotropic. To accurately estimate the gas-hydrate saturation of vertical fractures, anisotropic gas-hydrate analysis should be used. Such use is the focus of the next section.

Anisotropic Analysis

For anisotropic analysis of well logs, the properties chosen for the end members strongly affect the results. One important parameter is the porosity of the sediment surrounding fractures, but measured porosity is assumed to be the average of porosities of both fractures and water-saturated sediments surrounding the fractures. The porosity of water-saturated sediments alone is derived by using the following formula (Lee and Collett, 2009a):

$$\phi_2 = \frac{\phi_m - \eta}{1 - \eta}. \tag{18}$$

Equation 18 indicates that the porosity of water-saturated sediments is the same as the measured porosity, where there is no fracture (or gas hydrate). As the volume of the gas-hydrate-filled fracture increases, the porosity of the water-saturated sediments must decrease in order for the measured porosity to remain constant.

The porosity derived from the density log assumes that the densities of gas hydrate and water are the same. However, because the density of gas hydrate is less than that of water, the calculated porosity is not accurate for high-porosity sediments with high gas-hydrate saturations. To accurately compute porosity from a density log, the actual gas-hydrate saturation needs to be known. Consequently, estimating the gas-hydrate saturation and calculating porosity from the density log is an iterative process in which porosity is updated by using the estimated S_h as follows:

$$\phi_{new} = \phi_m \left[\frac{\rho_w - \rho_s}{\rho_w \left(1 - S_h\right) + \rho_h S_h - \rho_s} \right] \tag{19}$$

where ρ_w, ρ_h, and ρ_s are the density of the water, gas hydrate, and grains, respectively. The updated density porosity, ϕ_{new}, is used for ϕ_m in equation 18. However, for low gas-hydrate saturations, the porosity correction is insignificant and can be ignored.

Figure 7 shows the gas-hydrate saturations estimated for the fractured reservoir, if one assumes vertical fractures. For resistivity, values of $\phi_{w1} = 0.05$, $\lambda = 0$, and $\mu = 2$ are used for the fractures, and $\lambda = -0.01$, $\mu = 2$, and ϕ_{2w} calculated with equation 18 are used for the water-saturated sediments surrounding the fractures. For P-wave velocity, $V_{p1} = 3.77$ km/s, $V_{s1} = 1.96$ km/s, and $\rho_1 = 0.926$ g/cm^3 (Waite and others, 2009) are used for fractures, and P- and S-wave velocities for the surrounding water-saturated sediments are calculated by using porosity with equation 18 and $\alpha = 110(300/d)^{1.1}$. Note that the bulk and shear moduli and density of gas hydrate shown in table 1 yield a P-wave velocity of 3.77 km/s and

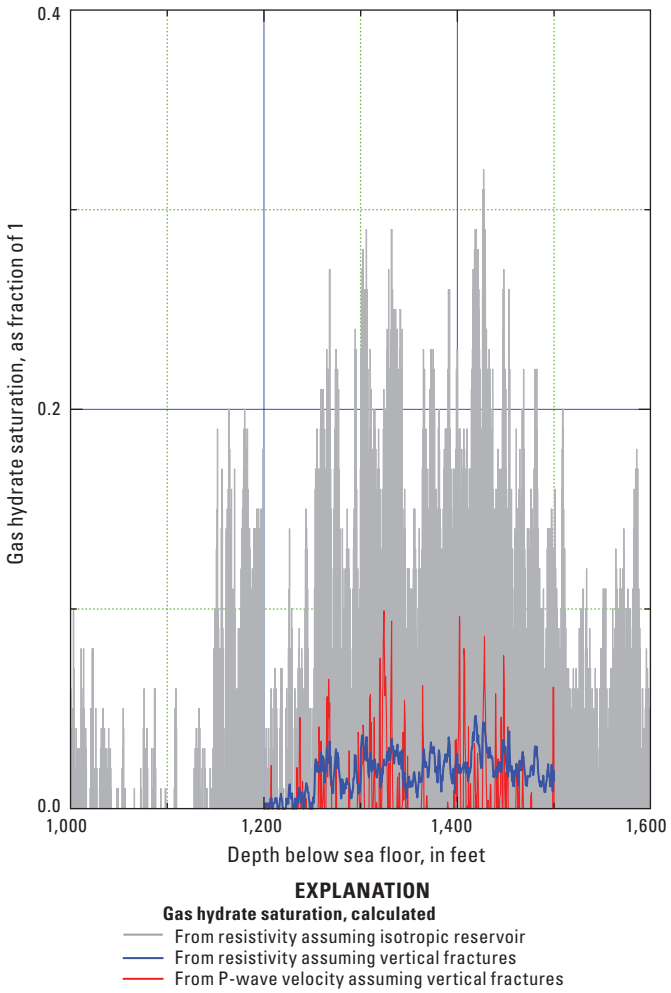

Figure 7. Gas-hydrate saturations estimated from resistivity by assuming isotropic gas-hydrate-bearing sediments, and from resistivity and P-wave velocity by assuming gas-hydrate-filled vertical fractures, at Gulf of Mexico well AC21–A.

an S-wave velocity of 1.96 km/s for pure gas hydrate. Gas-hydrate saturations estimated from resistivity by assuming vertical fractures (fig. 7) are much lower than those estimated by assuming isotropic gas-hydrate-bearing sediment (gray shading), but they agree well with those estimated from the P-wave velocity (fig. 7). Note that gas-hydrate saturations estimated from the P-wave velocities and by assuming isotropic gas-hydrate-bearing sediment are similar to those estimated by assuming anisotropic gas- hydrate-bearing sediment due to vertical fractures with low gas-hydrate saturations.

Results and Discussion

Gas Hydrate and Washout Models

The primary concern at well AC21–A is to determine whether there is gas hydrate in sands as predicted on the basis of seismic leading-peak analysis (Frye and others, 2009). It is generally accepted that logging measurements are accurate enough to estimate gas-hydrate saturation, because the effects of washouts on the logging measurements are automatically compensated for during well-log acquisition and processing. This assumption, however, is not valid at the AC21–A site, where there are large washouts in the clean sand intervals. Two models are presented to estimate gas-hydrate saturations in these sands. The first model assumes that there is no washout effect on the measured resistivity and P-wave velocity, thus indicating that there is little gas hydrate in the target sand reservoir. The second model, on the other hand, assumes that there is a substantial washout effect on the measured well logs, in which case there may be small to moderate amounts of gas hydrate in the target zone. However, because the gas-hydrate saturations estimated from resistivity and P-wave velocity differ by a factor of more than two at some intervals, quantifying the actual saturation is difficult.

All of the log measurements at well AC21–A are affected to some degree by the washout, although the washout effect differs from log to log. As an added complication, the distances of the various tools from the drill bit differ (for example, 35.45 ft for the SonicScope velocity tool and 60.51 ft for the ring resistivity tool). Therefore, the size of the washout could affect each logging tool differently. Also, because the distance between the source and receiver relative to the washout zone are different from tool to tool, the effect of the washout on the resistivity and velocity would be different. The vertical-fracture models for resistivity and velocity appear to be appropriate to qualitatively explain the anomalous measurements, but a determination of the size of the washout needed to account for the measurement discrepancies appears to be inaccurate. In the washout model, it is assumed that the size of the washout is proportional to the sand volume or inversely proportional to the shale volume (equation 16). However, the relation between the caliper log and the shale volume shows a lot of scattering. This scattering implies that equation 16 can qualitatively account for the washout effect but may not be accurate for quantitative analysis. Consequently, the proposed washout model can be

Table 1. Elastic constants used for velocity modeling of Alaminos Canyon well 21–A, Gulf of Mexico. Properties of gas hydrate from Waite and others (2009); remaining properties from Lee and Collett (2009a). The bulk and shear moduli of matrix ($_{ma}$) composed of quartz and clay (K_{ma} and μ_{ma}) are computed by using Hill's (1952) average equation.

[K, bulk modulus, μ, shear modulus, ρ, density; c, clay; h, gas hydrate; q, sand (quartz); w, water]

Bulk modulus (gigapascals)	Shear modulus (gigapascals)	Density (kilograms per cubic meter)
$K_q = 38$	$\mu_q = 44$	$\rho_q = 2{,}650$
$K_c = 20.9$	$\mu_c = 6.60$	$\rho_c = 2{,}580$
$K_h = 8.41$	$\mu_h = 3.54$	$\rho_h = 925$
$K_w = 2.29$	$\mu_w = 0$	$\rho_w = 1{,}000$

effectively used with the well logs to assess whether there is gas hydrate in the sediment's pore spaces, but the washout model should be used with caution to determine the gas-hydrate saturation quantitatively. This warning will be further emphasized in the following section.

Surface Seismic Data and Synthetic Seismograms

To determine the accuracy of the gas-hydrate saturations, velocity measurements unaffected by the borehole washout are required, and seismic data can provide this missing component. Figure 8*A* shows the synthetic seismograms generated from a variety of P-wave velocities (fig. 8*B*), by using a 50-hertz (Hz) Ricker wavelet along with the seismic trace intersecting well AC21–A. Although the wavelet for the surface seismic data is not identical to a 50-Hz Ricker wavelet, the following discussions are still valid.

Synthetic seismogram "a" (fig. 8*A*) is generated from measured P-wave velocities (black curve, fig. 8*B*). Because there is a shale break within the sand reservoir, the seismic response with a 50-Hz Ricker wavelet shows two peak-trough waveforms. The first peak indicates the top of the first reservoir (near 540 feet below the sea floor) and the second trough denotes the bottom of the second reservoir (near 632 feet below the sea floor). The seismic response between this peak and trough represents the seismic response for the entire sand reservoir including the shale break. The peak-trough travel time (that is, the two-way travel time from top to bottom of the entire sand reservoir) for synthetic seismogram "a" is 35 milliseconds (ms), which is about 4 ms slower than the peak-to-trough time measured on the surface seismic trace (fig. 8*A*). Because the peak-to-trough time is 4 ms slower on the synthetic seismogram than was measured on the surface seismic trace, the measured well log P-wave velocities are too low, requiring the synthetic seismogram to be "squeezed" in order to match the surface seismic data. Also, the relatively large amplitude of the peak-trough waveform observed for the sand reservoir in the surface seismogram is not present in synthetic seismogram "a," indicating that synthetic "a" is not a good match to the surface seismic trace.

Synthetic seismogram "b" (fig. 8*B*) is generated from the baseline P-wave velocities that were calculated by using washout-corrected porosities (fig. 2*B*), which assumed that only water is in the pore space (red curve, fig. 8*B* is the same as baseline P-wave velocity curve in fig. 6*B*). The peak-trough travel time measured for synthetic seismogram "b" is 32 ms, which is about 1 ms slower than the time measured on the surface seismic trace. Because these velocities are closely similar, the synthetic seismogram matches surface seismic data well. However, although the waveform for the target reservoir is similar to the surface seismic trace, the amplitudes of the first and second peaks do not match the surface seismic trace well. The 1-ms time difference between synthetic "b" and surface seismic trace indicates that there are likely some gas hydrates present in the sand reservoir, but only a small amount.

Synthetic seismogram "c" is generated by using P-wave velocities corrected for the washout effect and gas-hydrate saturation (fig. 8*B*, green curve). The peak-trough travel time is 31 ms, which is the same as the measured time. However, the peak-trough waveform shown on the surface seismogram differs slightly from that shown in synthetic seismogram "c"—the trough amplitude is much smaller than that of the surface seismogram.

Synthetic seismogram "d" is generated by using P-wave velocities calculated in turn by using gas-hydrate saturations estimated from resistivities that were corrected for the borehole washout effect (fig. 5*B*) and washout-corrected porosity (fig 2*B*) (blue curve, fig. 8*B*). Synthetic seismogram "d" matches the travel time of the surface seismic data and better matches the amplitudes of the surface seismic data than synthetic seismogram "c" does. This better agreement of amplitudes illustrates that at well AC21–A the borehole washout correction appears to be more accurate for resistivity than P-wave velocity. However, the trough amplitude at the base of the reservoir in synthetic seismogram "d" is slightly smaller than that of the surface seismic data.

Finally, synthetic seismogram "e" is generated by using a uniform gas-hydrate saturation of 13 percent in the sand reservoir (fig. 8*B*, brown curve). The amplitude variation of the synthetic for the reservoir interval fits remarkably well with that of the surface seismic data and provides the best match to the surface seismic data.

Gas Hydrate or Water?

The average gas-hydrate saturation estimated from resistivity with washout correction is about 13 percent, and the synthetic seismogram generated by assuming a uniform 13 percent gas- hydrate saturation agrees well with the surface seismic data as previously mentioned. How reliable is this small amount of gas-hydrate saturation estimated at well AC21–A? About 5 percent measurement error in the P-wave velocity and 10 percent error in the resistivity would yield about a 10 percent gas-hydrate-saturation error. Also, if there is about 10 percent error in porosity, there would be about 10 percent error in the saturation (M.W. Lee and T.S. Collett, unpub. data, 2011). In other words, if the in-place porosity is 34 percent instead of the 38 percent used in the analysis, no gas hydrate in the sand reservoir would be estimated from the P-wave velocity. Therefore, measurement errors of about 10 percent could have produced the gas-hydrate saturations estimated in this report, although the sand reservoir is water saturated.

What evidence supports gas hydrate rather than water in pore spaces in well AC21–1?

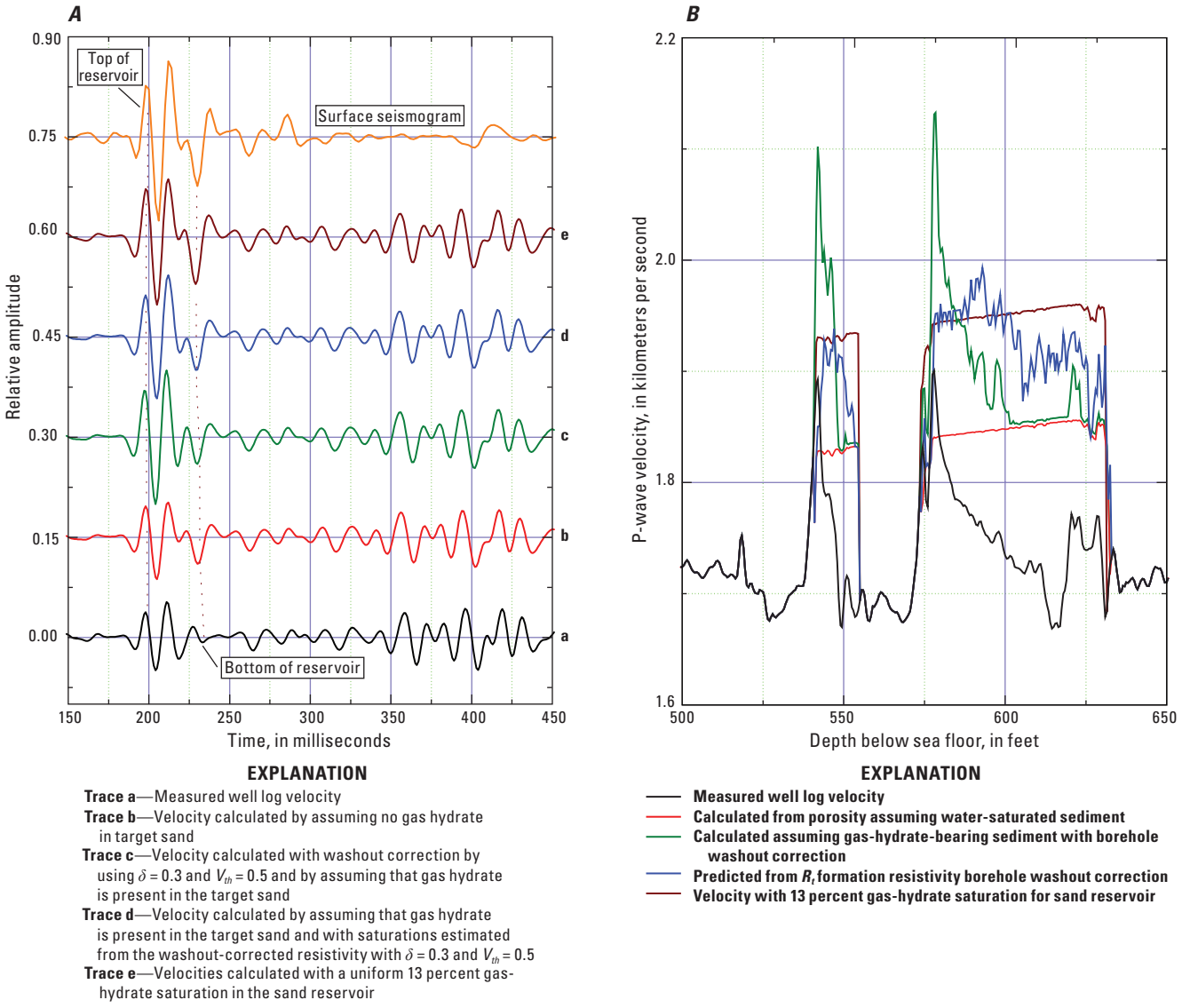

Figure 8. Various synthetic seismograms and their corresponding P-wave velocity models for a washed-out sand reservoir in Gulf of Mexico well AC21–A. *A*, Synthetic seismograms generated by using a 50-hertz Ricker wavelet and additional assumptions shown in Explanation. *B*, Velocity models produced by use of various measurements or calculations.

1. As observed during Gulf of Mexico JIP Leg II, P-wave velocities of sands without gas hydrate are much lower than the predicted velocities in water-saturated sediments because of severe washouts. The majority of well log velocities in the sand reservoir are lower than the predicted P-wave velocities (baseline velocities) of sands, as shown in figure 8*B*. However, at the top of the reservoirs, the measured P-wave velocities are higher than the calculated baseline velocities in water-saturated sediments and indicate smaller washouts, implying that some gas hydrate is holding the grains together. This relation also holds for the resistivity log.
2. Both P-wave velocity and resistivity, corrected for the effects of borehole washout, yielded positive gas-hydrate saturations. Synthetic seismogram "c," which was generated by using P-wave velocities corrected for the borehole washout, and synthetic seismogram "d," generated from P-wave velocities calculated by using gas-hydrate saturations estimated from borehole washout-corrected resistivity, are much closer to the trace of the surface seismogram than the synthetic seismogram that is generated by assuming no gas hydrate.

Although there is some suggestion of gas hydrate at well AC21–A, the result is not conclusive because of the uncertainties associated with measurements coupled with the uncertainties of rock physics model and parameters. However, it is reasonable to conclude that if gas hydrate is present, the saturation is probably less than 20 percent.

Characteristics of Reservoirs Containing High-Angle Fractures

To show the relation between the resistivity and the P-wave velocity measured at well AC21–A, the formation factor and P-wave velocities are plotted as a function of depth (fig. 9). The trend of the P-wave velocity is similar to that of the formation factor and resistivity except for the interval between 1,200 and 1,500 feet below the sea floor. As discussed previously, the measured formation factor in this interval is much higher than the calculated baseline resistivity (fig. 5), whereas the measured P-wave velocity is almost the same as the calculated baseline P-wave velocity (fig. 6).

Figure 10 shows a cross plot between the formation factor and the P-wave velocity at well AC21–A, along with modeled formation factor and P- and S-wave velocities for gas-hydrate-filled vertical and horizontal fractures. For comparison, the relation for an isotropic water-saturated model in clay-bearing sediments is also shown (fig. 10). Parameters used for the anisotropic resistivity model are $\phi_{w1} = 0.05$, $\mu_1 = 2$, $\lambda_1 = 0$, $\phi_{w2} = \phi_2 = 0.37$, $\mu_2 = 2$, $\lambda_2 = -0.01$, and $C_v = 0.6$. Parameters of the fracture for the velocity model are the same as before, and those for the host sediments are $V_{p2} = 1.99$ km/s, $V_{s2} = 0.59$ km/s, and $\phi_2 = 0.37$. Isotropic velocities of water-saturated sediments are modeled by using the modified Biot-Gassman theory by Lee (2002b) with $n = 1.5$ and $C_v = 0.36$, and resistivities are calculated by using equations 2 and 3 with $\mu = 2$ and $\lambda = -0.01$. Except for the samples between 1,200 and 1,500 feet below the sea floor, the relation between the P-wave velocity and formation factor follows that of the water-saturated sediments. On the other hand, the samples between 1,200 and 1,500 feet below the sea floor agree well with the relation predicted for vertical fractures. Because the change of formation factors with respect to the gas-hydrate saturation are large for the vertical fracture model and small for P-wave velocities at low saturations, gas-hydrate saturations estimated from resistivity have higher resolution for vertical fractures at low saturations. Consequently, gas-hydrate saturations estimated from resistivity (fig. 7) are more accurate than those estimated from the P-wave velocity.

To identify fractured reservoirs, both the resistivity and the P-wave velocity are required. If only P-wave velocity is measured, vertical fractures that contain only a small amount of gas hydrate would not have been identified. If only resistivity is measured, the gas-hydrate saturation would have been highly overestimated (Lee and Collett, 2009a).

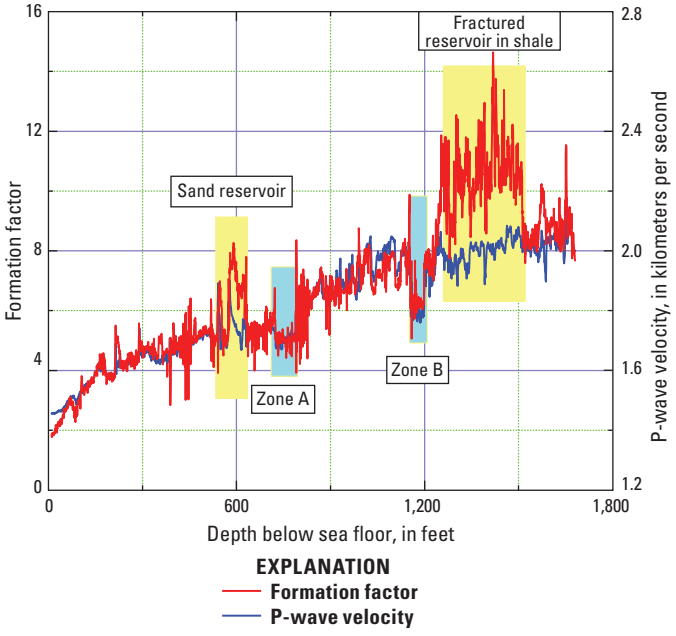

Figure 9. Formation factors and P-wave velocity measured at Gulf of Mexico well AC21–A. Formation factor and P-wave velocity plotted with respect to depth; four zones of interest are shaded.

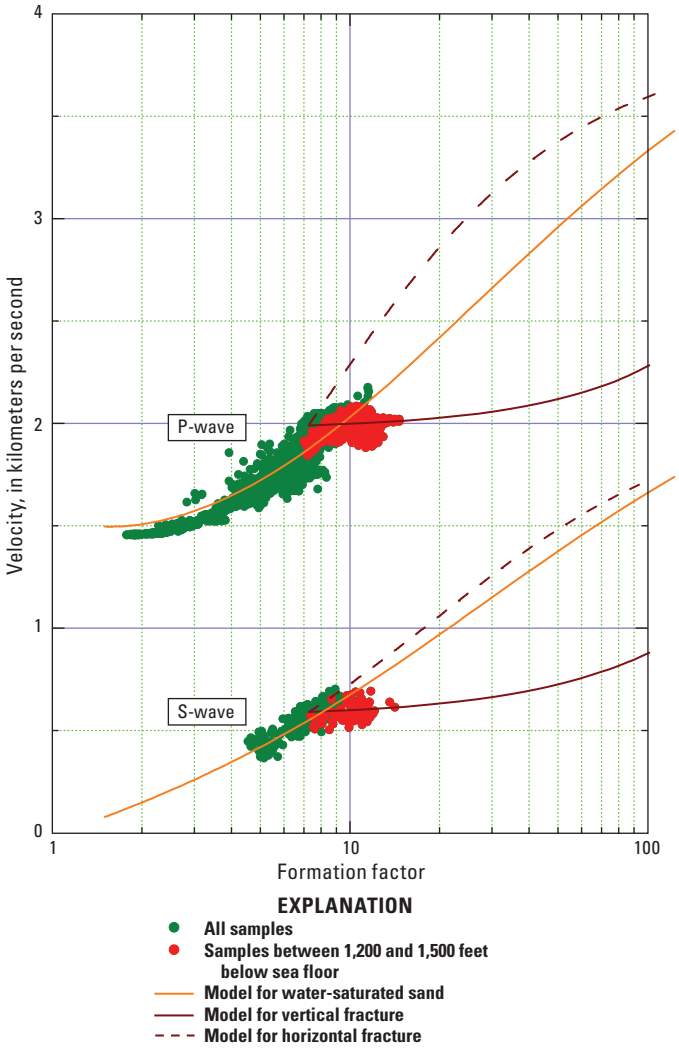

Figure 10. Cross plot of formation factor and velocity with modeled relation for fractures filled with gas hydrate and with water-saturated sediments at Gulf of Mexico well AC21–A.

Anomalous Zone A and Zone B

In zones A and B (fig. 9), measured P-wave velocities are similar to the calculated baseline velocities of water-saturated sediments (fig. 6), and measured resistivities are higher than calculated baseline resistivities (fig. 5). Saturations estimated from the resistivity are about 20 percent (figs. 5*A* and 5*B*), but saturations estimated from P-wave velocities are negligible (figs. 6*A* and 6*B*). Figure 11 shows shale volume and porosity and indicates that these zones are alternating silt and shale with porosities as much as 10 percent higher than those of adjacent sediments. Because of the different log responses for the resistivity and P-wave velocity, the pore saturants in zones A and B are not gas hydrate and could be some other hydrocarbons such as free gas or water with anomalous rock properties.

Higher porosities would be estimated if a higher matrix density is used or if the sediments contain some free gas (see appendix A). As discussed by Boswell and others (2009), the Frio sandstone at the Alaminos Canyon Block 818 (AC818), located south of well AC21–A (fig. 1), is known to contain volcanic glass. If so, porosities would be overestimated unless the low density of the volcanic glass is incorporated into the porosity calculations. Therefore, one reason for the higher porosities in zones A and B could be low-density grains such as volcanic glass in sediments.

If we assume that about 60 percent of the sediment's grains consists of volcanic glass with a density of 2.35–2.45 g/cm^3 (Shipley and Sarna-Wojcicki, 1982), then the expected grain density would be about 2.51 g/cm^3 instead of the 2.67 g/cm^3 used in this well-log analysis. If the grain density of 2.51 g/cm^3 is used for the porosity calculation at well AC21–A, equation A–2 (see appendix A) indicates that density porosities would be about 5 percent less than those shown in figure 11 for zone A.

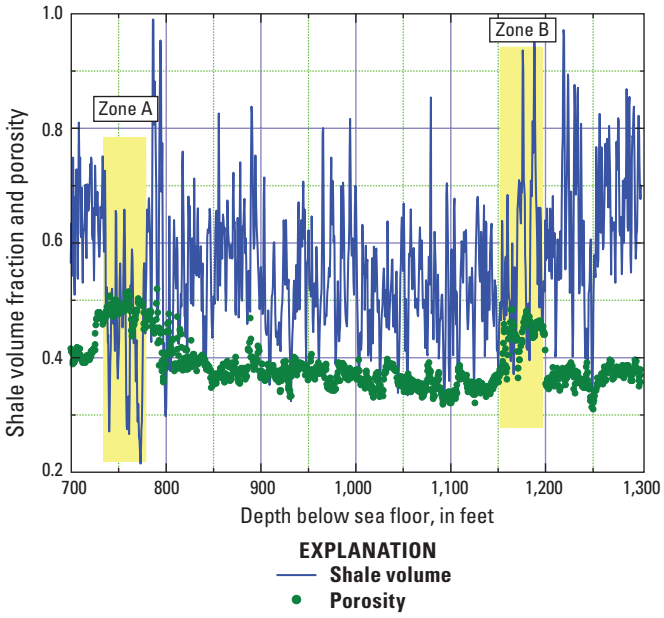

Figure 11. Shale volume fraction and porosity of zone A and zone B plotted with respect to depth.

If the porosities in zones A and B are overestimated by 5 percent, because of not accounting for the volcanic glass in the grains, the saturation estimated from the resistivity would be near zero, but the calculated P-wave velocities are slightly higher than the measured velocity. If the bulk and shear moduli of volcanic glass are smaller than those of sand, this model could explain the anomalous velocities calculated for zones A and B. P-wave velocities for zones A and B (fig. 12) are modeled by using reduced porosity with assumed bulk and shear moduli of volcanic glass (70 percent of the bulk and shear moduli of sand are assumed for volcanic glass) to simulate the effect of volcanic glass. The calculated P-wave velocities agree well with those measured. For comparison, calculated velocities of water-saturated sediments with reduced porosity but with the same bulk and shear moduli of sand are much higher than measured velocities (fig. 12).

Another possible cause for the anomalous velocities and resistivities observed in zones A and B is that free gas is present in the zones, and that the anomalously high porosities

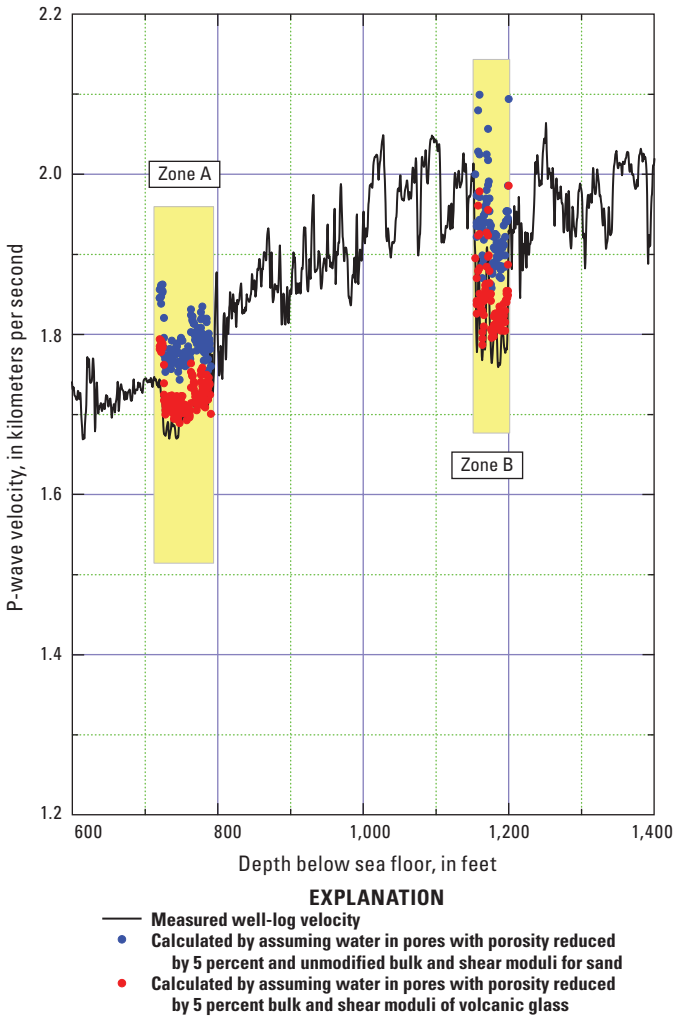

Figure 12. Measured and calculated P-wave velocities for zones A and B by assuming water-wet sediments. Modified bulk and shear moduli (red dots) simulate the effect of volcanic glass in the sediment.

are caused by not accounting for a free-gas effect on the porosity calculation (appendix A). Free gas is sometimes observed within the gas-hydrate stability zone (Lee and Collett, 2006). To have a strong gas effect on porosity, gas saturation should be high. However, on the basis of measured P-wave velocity and the resistivity, high gas saturations at well AC21–A are not possible. Therefore, it may be that a small amount of free gas is present in zones A and B under the assumption that high porosities in zones A and B are caused by the presence of volcanic glass. A small amount of free gas, less than a few percent, would not affect the porosity but would markedly affect P-wave velocity. P-wave velocities (fig. 13) were calculated at the logging frequency (4.5 kilohertz (kHz)) by assuming free gas in zone A (0.4 percent) and in zone B (1.5 percent) with 5 percent reduced porosity and by using the White (1975) model. Assuming a small amount of free gas also may explain the anomalous P-wave velocity and resistivities for zones A and B quite well (fig. 13).

It is known that partially gas-saturated sediments are dispersive and that the P-wave velocities of such sediments at seismic frequencies are noticeably different from those at logging frequencies (Lee and Collett, 2009b). Figure 13 shows the P-wave velocity calculated at 100 Hz (that is, at seismic frequency) using the same parameters used for the well log velocity from the White (1975) model. The average measured velocity for zones A and B is 1.744 km/s. The average velocity calculated for partially gas-saturated sediments at 4.5 kHz is 1.742 km/s, whereas it is 1.398 km/s at 100 Hz. Therefore, the arrival time at the base of zone B in the synthetic seismogram with free gas is 10 ms later than that generated without free gas. Two calculated synthetic seismograms show one with and one without free gas in zones A and B (fig. 14). The arrival times at the bases of zones A and B in the synthetic generated without free gas (this seismogram is identical to synthetic seismogram "e," fig. 8*A*) agree well with the surface seismic data, but the base of zone B in the synthetic seismogram generated with free gas is 10 ms later than the surface seismic data. Although high attenuation is expected for the partially gas-saturated sediments, the synthetic without free gas is a better match to the surface seismic trace in terms of both arrival time and amplitude (fig. 14). Along with the analysis of the washed-out sand reservoir, the analysis of zones A and B illustrates the importance of using surface seismic data to constrain the interpretation of well log data and to validate rock physics models.

Properties similar to those observed in zone A were also observed at the same stratigraphic interval in the well logs of well AC21–B, 7,740 ft east of well AC21–A (fig. 1). Therefore, the anomalous measurements that were observed in zones A and B are not likely caused by measurement error. To fully understand these anomalous zones, more data including core data are required. However, on the basis of currently available information, it is plausible to interpret that zones A and B contain water-saturated sediment having anomalously low matrix density and having bulk and shear moduli such as for volcanic glass.

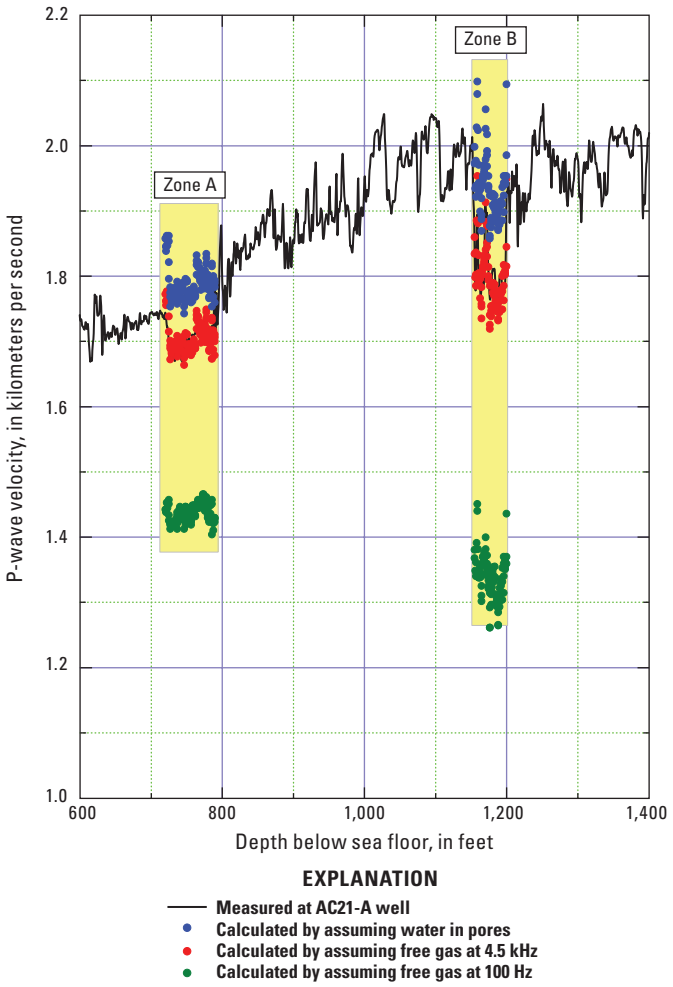

Figure 13. Measured and calculated P-wave velocities in zones A and B, by assuming free gas in pore spaces. Blue dot, P-wave velocity calculated by using porosity reduced by 5 percent without free gas. Red dot, P-wave velocity calculated at a dominant frequency of 4.5 kilohertz by using porosity reduced by 5 percent with a free gas saturation of 0.4 percent in zone A and 1.5 percent in zone B. Green dot, P-wave velocity calculated at 100 hertz by using porosity reduced by 5 percent with a free gas saturation of 0.4 percent in zone A and 1.5 percent in zone B.

Leading Peak and Gas Hydrate Prospecting

At the Alaminos Canyon site, Frye and others (2009) used the leading peak of the reflection at the top of the sand reservoir as an indicator of gas hydrate. This interpretation is based mainly on the model developed for the Alaska North Slope (Inks and others, 2009; Lee and others, 2009), where the impedance of water-saturated sand (no gas hydrate) is less than that of the bounding shale. In the case of the North Slope model, the top of the water-saturated sand reservoir is represented as a trough in the seismic section. If gas hydrate is present in the sand, then the amplitude increases in a positive manner as gas-hydrate saturation increases, eventually causing the trough to become a peak at high saturations. In

this case, the leading peak is a good indicator of gas hydrate, although the interpretation critically depends on knowing local properties of the sediment.

Figure 8*B* shows P-wave velocities of the sand reservoir without gas hydrate (red curve) and bounding shale. On the basis of this figure and other logs, it is assumed that the P-wave velocity, clay volume, and porosity of bounding shale are 1.71 km/s, $C_v = 0.36$, and $\phi = 0.4$, respectively. For the reservoir sand not containing gas hydrate, the P-wave velocity, clay volume, and porosity are assigned as 1.84 km/s, $C_v = 0.1$, and $\phi = 0.38$, respectively.

The calculated P-wave velocity and reflection coefficient of the top of the reservoir with respect to gas-hydrate saturation were obtained by using equations 5–8 and assuming $\alpha = 53$ (fig. 15*A*). P-wave velocity increases from 1.84 km/s at zero saturation to 2.8 km/s at 80 percent gas-hydrate saturation, and the reflection coefficient increases from 0.065 to 0.259. Note that the reflection coefficient produced by water-wet sand is positive and comparable to the reflection coefficient of 0.088 that is generated for sand with a 13-percent gas-hydrate saturation (best model for well AC21–A). Therefore, interpreting the leading peak as an indicator of the gas-hydrate accumulation is inaccurate at well site AC21–A. It is possible to interpret the leading peak as an indicator of gas hydrate for deeper reservoirs (below approximately 1,500 feet below the sea floor), because (according to a model by Gregory (1977) impedance reverses between the shale and sand. However, use caution when the leading peak is used as a gas-hydrate indicator.

Because the seismic data represent the constructive and destructive interferences of reflections owing to finite seismic bandwidth, the interpretation of amplitude is more complicated, and a thin-bed analysis proposed by Lee and others (2009) is applicable to estimate thickness and gas-hydrate saturations. The amplitude variation with respect to bed thickness for a given gas-hydrate saturation (fig. 15*B*) was obtained by using the model shown in figure15*A* with a 50-Hz Ricker wavelet. Also shown is the amplitude variation with respect to saturation for a constant thickness. Thickness of D = 15 ft represents the upper sand body and D = 60 ft represents the lower sand body. The upper sand body is too thin for a dominant frequency of 50 Hz, and the apparent two-way travel-time thickness (mapped time between peak and trough amplitudes) is almost constant regardless of change in gas-hydrate saturation. Consequently, it is difficult to uniquely determine the saturation and reservoir thickness from the mapped seismic amplitude and time thickness; that determination requires a dominant frequency much higher than 50 Hz to resolve the upper sand reservoir. On the other hand, the lower sand body is thick enough to permit interpretation of variation in amplitude and time thickness in terms of gas-hydrate saturation and reservoir thickness (Inks and others, 2009; Lee and others, 2009) by using a dominant frequency of 50 Hz.

The thin-bed interpretation for gas-hydrate prospecting proposed by Lee and others (2009) is accurate for an isolated reservoir. At well AC21–A, two reflections from two

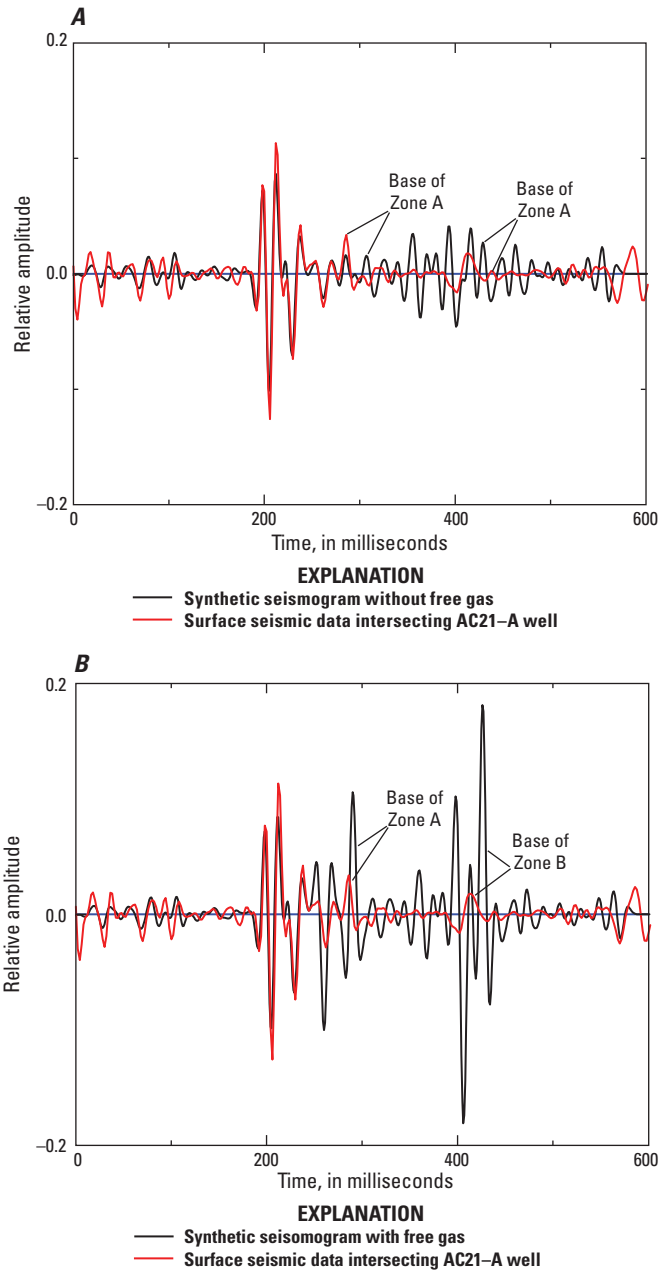

Figure 14. Synthetic seismograms and surface seismic data intersecting Gulf of Mexico well AC21–A. *A*, Synthetic seismogram generated without free gas (also synthetic seismogram "e" in figure 8*A*). *B*, Synthetic seismogram generated with velocities calculated with free gas. P-wave velocities are calculated at 100 hertz with a free gas saturation of 0.4 percent in zone A and 1.5 percent in zone B (same as fig. 13, green dots).

sand reservoirs interfere, so amplitude and time thickness interpretation is not simple. However, by comparing the second peak and trough amplitudes (corresponding with the reflection from the lower sand body) shown in the synthetic seismograms "b" and "e" (fig. 8*A*), it appears that interpreting the amplitude and time in terms of saturation and thickness from seismic data having a dominant frequency around 50 Hz is possible for the lower sand body at well site AC21–A.

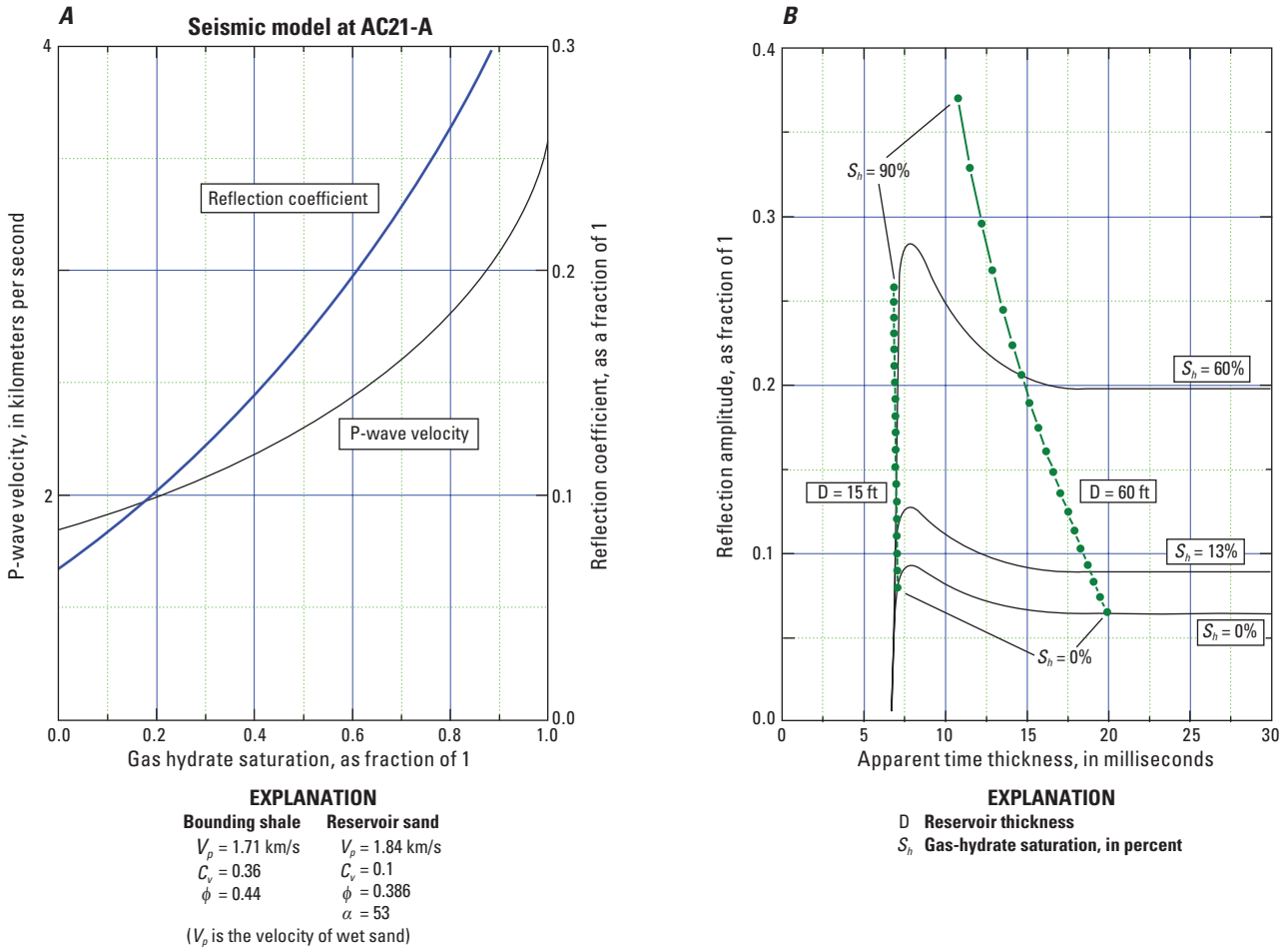

Figure 15. Thin-bed modeling used for gas-hydrate prospecting. *A*, P-wave velocity of the sand reservoir and reflection coefficient at the top of the reservoir with respect to the gas-hydrate saturation by using model parameters shown in the figure. *B*, Reflection amplitude as a function of apparent two-way travel-time thickness of reservoir at gas-hydrate saturations 0, 12, and 60 percent (solid curves) and at given true reservoir thicknesses of 15 and 50 ft by using a 50-hertz Ricker wavelet. True thickness of the sand reservoir (in feet) is converted into apparent two-way travel time using the modeled P-wave velocity shown in figure 15*A*. porosity; C_v, clay volume; V_p, P-wave velocity; α, consolidation parameter; S_h, gas-hydrate saturation; D, thickness of reservoir.

Summary and Conclusions

Two models are presented to assess the presence of gas hydrate at the Gulf of Mexico well site AC21–A. One model assumes no borehole washouts that could affect the resistivity and velocity well logs, and the other model assumes that resistivity and velocity well logs were affected substantially by washouts. If we assume no washouts and that the measured resistivity and velocities with modified porosity are accurate, this model yields negligible gas hydrate in the target sands. However, this model does not fit the surface seismic data at this location because (1) the two-way travel time from the top of the reservoir to the bottom of the reservoir is approximately 4 milliseconds longer than the travel time measured on the surface seismic trace intersecting well AC21–A, and (2) the waveforms of the surface seismic trace are noticeably different from synthetic waveforms generated from the well logs. On the other hand, if it is assumed that a washout affected both the resistivity and P-wave velocity and that the washout effect is accounted for in the measured well log values, this model yields gas-hydrate saturation of less than about 20 percent in the target sands. The seismic model that assumes that a target sand that contains gas hydrate at 13 percent saturation fits the surface seismic data best. Also, if gas-hydrate saturations estimated from the resistivity with borehole-washout corrections applied are inserted into the acoustic equation, the synthetic seismogram using this velocity model (synthetic seismogram "d" in figure 8*A*) agrees remarkably well with the surface seismic data.

During Gulf of Mexico Gas Hydrate Joint Industry Program Leg II logging-while-drilling expedition, it was observed that minimal borehole enlargement (washout) occurred in gas-hydrate-bearing and clay-bearing sediments, whereas large washouts were observed in clean sands not containing gas hydrates. In well AC21–A, some parts of the

target sand interval were affected less by washouts than were other intervals of the well. These smaller washouts, which are in the target sand zones where the measured resistivity of 2 ohm-meters and the P-wave velocity of 1.9 kilometers per second are slightly higher than those calculated baseline values, may be additional qualitative indicators of gas hydrates.

This study demonstrates the importance of using surface seismic data to constrain gas-hydrate saturation estimated from the well log data where severe washouts have degraded well log quality. It is essential to assess the accuracy of the well log interpretation by using the seismic data for well AC21–A. Although there is some evidence of gas hydrate at well AC21–A, it is not conclusive because of the inherent uncertainties associated with the log measurements coupled with uncertainties of rock physics models and parameters. However, it is reasonable to state that if gas hydrate exists at site AC21–A, the gas-hydrate saturation is probably low, less than 20 percent.

Because the impedance of wet sand at well AC21–A is higher than that of the bounding shale, the reflection amplitude from the top of the wet sand reservoir is a peak. Therefore, caution is required in interpreting the peak amplitude in the seismic data as an indicator of gas hydrate.

Gas-hydrate-filled vertical fractures in clay-bearing sediments were also observed in the Alaminos Canyon well and, by using anisotropic analysis of resistivity and P-wave velocity, gas- hydrate saturations were estimated to be about 5 percent of the pore space. To identify gas hydrate in vertical fractures, both velocity and resistivity data are required. Isotropic resistivity analysis for the vertical fracture overestimates gas-hydrate saturation by a factor of about 4 or 5. Because the resistivity change with respect to the fracture volume is much higher than that of P-wave velocity at low gas-hydrate saturations, resistivity appears to be more accurate for estimating saturations in vertical fractures. However, because isotropic and anisotropic analyses of P-wave velocity for low gas-hydrate saturations are similar, an isotropic analysis of the P-wave velocity can be used to estimate gas-hydrate saturations for high-angle fractures with low gas-hydrate saturations.

Two anomalous zones were observed in well AC21–A that have porosities more than 10 percent as larger as those of the surrounding sediments; these zones also have resistivity higher than the baseline resistivity but a P-wave velocity similar to the baseline velocity. One plausible interpretation is that these two anomalous zones consist of water-saturated sediments that contain volcanic glass having low matrix density and bulk and shear moduli.

Well logs contain important information that can be used to estimate the amount of in-place gas hydrate. However, accurate estimates cannot be achieved unless borehole washout correction is applied to measured logs, and different types of gas hydrate reservoirs, such as isotropic sand reservoirs and anisotropic clay-bearing sediments, are identified. It is also emphasized that surface seismic data are important to constrain the interpretation of the well log data and to validate rock physics models.

Acknowledgments

I thank W.F. Agena and K.A. Lewis for their many helpful comments and suggestions and T.S. Collett for his continuous support of this investigation. This work was funded by the U.S. Department of Energy and the Energy Resources Program of the U.S. Geological Survey. Data used in this paper were provided by the Department of Energy-sponsored Gulf of Mexico Gas Hydrate Joint Industry Project Leg II.

References Cited

Archie, G.E., 1942, The electrical resistivity log as an aid in determining some reservoir characteristics: Journal of Petroleum Technology, v. 1, p. 55−62.

Arp, J.J., 1953, The effect of temperature on the density and electrical resistivity of sodium chloride solutions: Petroleum Transaction, American Institute of Mining, Metallurgical, and Petroleum Engineers, v. 198, p. 327−330.

Asquith, George, and Krygowski, D., 2004, Porosity logs, *in* Asquith, G., and Krygowski, D., (eds.), Basic well log analysis: American Association of Petroleum Geologists Method in Exploration 16, p. 37–76.

Boswell, Ray, Shelander, D., Lee, M., Latham, T., Collett, T., Guerin, G., Modridis, G., Reagan, M., and Goldberg, D., 2009, Occurrence of gas hydrate in Oligocene Frio sands—Alaminos Canyon Block 818, northern Gulf of Mexico: Marine and Petroleum Geology, v. 26, p. 1499−1512.

Collett, T.S., Boswell, R., Mrozewski, S., Guerin G., Cook, A., Frye, M., Shedd, W., and McConnell, D., 2009, Gulf of Mexico Gas Hydrate Joint Industry Project Leg II—Operational summary: Proceedings of the Drilling and Scientific Results of the 2009 Gulf of Mexico Gas Hydrate Joint Industry Project Leg II, *http://www.netl.doe.gov/technologies/oil-gas/publications/Hydrates/2009Reports/OpSum.pdf* , 27 p. Accessed 8-10-2011.

Collett, T.S., and Ladd, J., 2000, Detection of gas hydrate with downhole logs and assessment of gas hydrate concentrations (saturations) and gas volumes on the Blake Ridge with electrical resistivity log data, *in* Paull, C.K., Matsumoto, R., Wallace, P.J., and Dillon, W.P. (eds.), Proceedings of the Ocean Drilling Programs, Scientific Results, 164: College Station, Texas (Ocean Drilling Program), p. 179−191.

Ecker, Christine, Lumlet, D., Dvorkin, J., and Nur, A., 1998, Sediments within gas hydrates: Internal structure from seismic AVO: Geophysics, v. 63, p. 1659−1669.

Frye, Matthew, Shedd, W., Godfriaux, P., Collett, T, Lee, M., Boswell, R., Dufrene, R., and McConnell, D., 2009, Gulf of Mexico Gas Hydrate Joint Industry Project Leg II—Alaminos Canyon 21 site summary: Proceedings of the Drilling and Scientific Results of the 2009 Gulf of Mexico Gas Hydrate Joint Industry Project Leg II, at URL *http://www.boem.gov/uploadedFiles/BOEM/Oil_and_Gas_Energy_Program/Resource_Evaluation/Gas_Hydrates/JIP_AlaminosCanyon21_SiteSum.pdf* , 28 p. Accessed 8–10–2011.

Gregory, A.R., 1977, Aspect of rock physics from laboratory and log data that are important to seismic interpretation, in Payton, C.E. (ed.), Seismic stratigraphy—Applications to hydrocarbon exploration: American Association of Petroleum Geologists Memoir 26, p. 15−46.

Guerin, Gilles, Goldberg, D., and Meltser, A., 1999, Characterization of in situ elastic properties of gas hydrate-bearing sediments on the Blake Ridge: Journal of Geophysical Research, v. 104, p. 17,781−17,795.

Hearst, J.R., Nelson, P.H., and Paillett, F.L, 2000, Well logging for physical properties—A handbook for geophysicists, geologists and engineers: New York, John Wiley and Sons, 484 p.

Helgerud, M.B., Dvorkin, J., Nur, A., Sakai, A., and Collett, T., 1999, Elastic-wave velocity in marine sediments with gas hydrates—Effective medium modeling: Geophysical Research Letters, v. 26, p. 2021−2024.

Hill, R., 1952, The elastic behavior of crystalline aggregate: Proceedings of Physical Society of London, A65, p. 349−354.

Hutchinson, D.R., Boswell, R., Collett, T.S., Dai, J., Dugan, B., Frye, M., Jones, E., McConnell, D., Rose, K., Ruppel, C., Shedd, W., Shelander, D., and Wood, W., 2009, Gulf of Mexico Gas Hydrate Joint Industry Project Leg II—Walker Ridge 313 site selection: Proceedings of the Drilling and Scientific Results of the 2009 Gulf of Mexico Gas Hydrate Joint Industry Project Leg II, at URL *http://www.netl.doe.gov/technologies/oil-gas/publications/Hydrates/2009Reports/WR313SiteSelect.pdf* , 35 p. Accessed 8-10-2011.

Inks, Tanya, Lee, M., Agena, W., Taylor, D., Collett, T., Hunter, R., and Zyrianova, M., 2009, Prospecting for gas hydrate accumulations using 2D and 3D seismic data, Milne Point, North Slope, Alaska, *in* Collett, T.S., Johnson, A., Knapp, C., and Boswell, R. (eds.), Natural gas hydrates—Energy resource potential and associated geologic hazards: American Association of Petroleum Geologists Memoir 89, 29 p.

Jakobsen, M., Hudson, J.A., Minshull, T.A., and Singh, S.C., 2000, Elastic properties of hydrate-bearing sediment using effective medium theory: Journal of Geophysical Research, v. 105, p. 561−577.

Kennedy, W.D., and Herrick, D.C., 2004, Conductivity anisotropy in shale-free sandstone: Petrophysics, v. 45, p. 38−58.

Kolterman, C.E., and Gorelick, S., 1995, Fractional packing model for hydraulic conductivity derived from sediment mixtures: Water Resources Research, v. 31, p. 3283−3297.

Lee, M.W., 2002a, Biot-Gassmann theory for velocities of gas-hydrate-bearing sediments: Geophysics, v. 67, p. 1711−1719.

Lee, M.W., 2002b, Modified Biot-Gassmann theory for calculating elastic velocities for unconsolidated and consolidated sediments: Marine Geophysical Researches, v. 23, p. 403−412.

Lee, M.W., 2005, Proposed moduli of dry rock and their application to predicting elastic velocities of sandstones: U.S. Geological Survey Scientific Investigations Report 2005−5119, 14 p.

Lee, M.W., 2006, A simple method of predicting S-wave velocity: Geophysics, v. 71, p. F161−F164.

Lee, M.W., 2008, Models for gas hydrate-bearing sediments inferred from hydraulic permeability and elastic velocities: U.S. Geological Survey Scientific Investigations Report 2008−5219, 15 p.

Lee, M.W., 2009, Anisotropic velocities of gas hydrate-bearing sediments in fractured reservoirs: U.S. Geological Survey Scientific Investigations Report 2009−5141, 13 p.

Lee, M.W., 2011, Connectivity equation and shaly sand correction for electrical resistivity log: U.S. Geological Survey Scientific Investigations Report 2011−5005, 9 p.

Lee, M.W., and Collett, T.S., 2006, Gas hydrate and free gas saturations estimated from velocity logs on Hydrate Ridge, offshore Oregon, U.S.A., *in* Trehu, A.M., Bohrmann, G., Torres, M.E., and Colwell, F.S. (eds.), Proceedings of the Ocean Drilling Program Scientific Results, v. 204, 25 p. (online) [*http://www-odp.tamu.edu/publications/204_SR/103/103.htm*]

Lee, M.W., and Collett, T.S., 2009a, Gas hydrate saturations estimated from fractured reservoir at Site NGHP-10-10, Krishna-Godavari Basin, India: Journal of Geophysical Research, v. 114, B07102, doi:10.1029/208JB006237, 13 p.

Lee, M.W., and Collett, T.S., 2009b, Unique problems associated with seismic analysis of partially gas-saturated unconsolidated sediments: Marine and Petroleum geology, v. 26, p. 775−781.

Lee, M.W., Collett, T.S., and Inks, T.L., 2009, Seismic attribute analysis for gas-hydrate and free-gas prospects on the North Slope of Alaska, *in* Collett, T.S., Johnson, A., Knapp, C., and Boswell, R., eds., Natural gas hydrates—Energy resource potential and associated geologic hazards: American Association of Petroleum Geologists Memoir 89, 14 p.

Lee, M.W., and Waite, W.F., 2008, Estimating pore-space gas hydrate saturations from well-log acoustic data: Geochemistry, Geophysics, Geosystems, v. 9, Q07008, doi:10,1029/2008GC002081, 8 p.

Marion, Dominique, Nur, A., Yin, H., and Han, D., 1992, Compressional velocity and porosity in sand-clay mixture: Geophysics, v. 57, p. 554−563.

Mindlin, R.D., 1949. Compliance of elastic bodies in contact: Journal of Applied Mechanics Transaction, v. 71, p. 259−268.

Montaron, Bernard, 2009, Connectivity theory—A new approach to modeling non-Archie rocks: Petrophysics, v. 50, p. 102−115.

Pratson, L.F., Stroujkova, A., Herrick, D., Boadu, F., and Malin, P., 2003, Predicting seismic velocity and other rock properties from clay content only: Geophysics, v. 68, p. 1847−1856.

Pride, S.R., Berryman, J.G., and Harris, J.M., 2004, Seismic attenuation to wave-induced flow: Journal of Geophysical Research, v. 109, B01201, doi:10.1029/2003JB002639.

Shedd, William, Hutchinson, D., Boswell, R., Collett, T., Dai, J., Dugan, B., Frye, M., Jones, E., McConnell, D., Rose, K., Ruppel, C., Shelander, D., and Wood, W., 2009, Gulf of Mexico Gas Hydrate Joint Industry Project Leg II— East Breaks 991 and Alaminos Canyon 21 site selection: Proceedings of the Drilling and Scientific Results of the 2009 Gulf of Mexico Gas Hydrate Joint Industry Project Leg II, at URL *http://www.netl.doe.gov/technologies/oil-gas/publications/Hydrates/2009Reports/AC21SiteSelect.pdf* , 18 p. Accessed 8-10-2011.

Shipley, S., and Sarna-Wojcicki, A.M., 1982, Distribution, thickness, and mass of late Pleistocene and Holocene tephra from major volcanoes in northwestern United States—A preliminary assessment of hazards from volcanic ejecta to nuclear reactors in the Pacific Northwest: U.S. Geological Survey Miscellaneous Field Studies Map MF−1435.

Waite, W.F., Santamarina, J.C., Cortes, D.D., Dugan, B., Esponoza, D.N., Germaine, J., Jang, J., Jung, J., Kneafsey, T., Shin, H.S., Soga, K., Winters, W., and Yun, T.-S., 2009, Physical properties of hydrate-bearing sediments: Review of Geophysics, v. 47, RG4003, doi:10/1029/2008RG200279.

White, J.E., 1965, Seismic waves-radiation, transmission, and attenuation: New York, McGraw-Hill, 302 p.

White, J.E., 1975, Computed seismic speeds and attenuation in rocks with partial gas saturation: Geophysics. v. 40, p. 224−232.

Zimmer, M.A., 2003, Seismic velocities in unconsolidated sands—Measurements of pressure, sorting, and compaction effects: Palo Alto, Calif., Stanford University, Ph.D. dissertation, 204 p.

Appendix A. Porosity

Porosity is the most important parameter in estimating gas-hydrate and free gas saturations, particularly for sediments with low porosity and small amounts of gas hydrate or free gas. Porosity derived from the bulk density measurement is calculated assuming a two-component system consisting of water and matrix. Errors in matrix density or a pore saturant other than water affect the calculated porosity. Generally, free gas in the pore space causes overestimates of porosity unless free gas is included in the calculations. Free gas in sediments produces the well-known density–neutron porosity crossover (Asquith and Krygowski, 2004). In order to accurately calculate porosity, a three-component system consisting of the grains, water, and free gas must be used.

Porosity (ϕ) can be estimated from bulk density (ρ_b) logs by using the following equation:

$$\phi = \frac{\rho_{ms} - \rho_b}{\rho_{ma} - \rho_g S_g - \rho_w (1 - S_g)} \tag{A–1}$$

where ρ_{ma}, ρ_w, and ρ_g are the densities of the sediment grains or matrix, water, and gas, respectively, and S_g is the gas saturation. Two different porosities can be calculated from the bulk density log and compared: one by assuming a two-component system (grains and water) and other by assuming a three-component system (grains, water, and gas). The effect of gas hydrate in calculating porosity is ignored here because the effect of the gas hydrate on porosity is accounted for by equation 19.

A porosity error ($\Delta\phi$) owing to error in the grain density ($\Delta\rho_{ma}$) can be written by using equation A–1 as follows:

$$\Delta\phi = \frac{(1 - \phi)}{\left[\rho_{ma} - \rho_g S_g - \rho_w (1 - S_g)\right]} \Delta\rho_{ma} \approx \frac{(1 - \phi)}{\left[\rho_{ma} - \rho_w (1 - S_g)\right]} \Delta\rho_{ma} \tag{A–2}$$

The approximation in equation A–2 is appropriate because the density of gas is negligible compared with the density of grains. Equation A–2 indicates that the porosity error increases as the error in the grain density increases. In other words, a higher grain density overestimates porosity from the density log. Therefore, the anomalously high porosities at zones A and B shown in in figure 11 (main report) could be caused by using a grain density that is too high.

If free gas is present in the sediment but the two-component porosity equation is used, porosity will be overestimated. This overestimation becomes apparent by calculating the ratio of three-component porosity to two-component porosity, given by the following:

$$\phi_R = \frac{\phi_{cg}}{\phi_{cw}} = \frac{\rho_{ma} - \rho_w}{\rho_{ma} - S_g \rho_g - (1 - S_g)\rho_w} \approx 1 - \frac{S_g \rho_w}{\rho_{ma} - \rho w} \tag{A–3}$$

where ϕ_{cg} is the three-component porosity and ϕ_{cw} is the two-component porosity. From equation A–3, it becomes apparent that, if gas saturation is high and the two-component system is used, porosity will be overestimated and the magnitude of the overestimation increases as gas saturation increases.

Publishing support provided by:
Denver Publishing Service Center, Denver, Colorado

For more information concerning this publication, contact:
Center Director, USGS Central Energy Resources Science Center
Box 25046, Mail Stop 939
Denver, CO 80225
(303) 236-1647

Or visit the Central Energy Resources Science Center Web site at:
http://energy.cr.usgs.gov/

This publication is available online at:
http://pubs.usgs.gov/sir/2012/5046/